

Absorption-Line Systems and Galaxies in Front of the Second Brightest Quasar, PHL 1811¹

Edward B. Jenkins, David V. Bowen, Todd M. Tripp

*Princeton University Observatory
Princeton, NJ 08544-1001*

`ebj@astro.princeton.edu, dvb@astro.princeton.edu, tripp@astro.princeton.edu`

Kenneth R. Sembach²

*Department of Physics and Astronomy, Johns Hopkins University
3400 N. Charles St., Baltimore, MD 21218*

`sembach@stsci.edu`

Karen M. Leighly

*University of Oklahoma Dept. Physics and Astronomy,
440 W. Brooks St., Norman, OK 73019*

`leighly@ou.edu`

Jules P. Halpern

*Department of Astronomy, Columbia University
550 W. 120th St., Mail Code 5230, New York, NY 10027-6601*

`jules@astro.columbia.edu`

J. T. Lauroesch

*Department of Physics and Astronomy, Dearborn Observatory
2131 Sheridan Road, Northwestern University, Evanston, IL 60208*

`jtl@elvis.astro.northwestern.edu`

ABSTRACT

The extraordinarily bright quasar PHL 1811 at a redshift $z_{\text{em}} = 0.192$ provides an attractive opportunity to use ultraviolet absorption-line spectroscopy to study the properties of gas systems in the local universe. A short (11.3 ksec), exploratory spectrum of this object was obtained by the *Far Ultraviolet Spectroscopic Explorer (FUSE)* with $\text{S/N} = 20$ per $\lambda/20,000$ resolution element over the most relevant portions of the coverage from 907 to 1185 Å. This spectrum reveals 7 extragalactic absorption systems, one of which is a Lyman limit system at $z_{\text{abs}} = 0.08093$ with $17.5 < \log N(\text{H I}) < 19.5$. Three of the remaining systems have z_{abs} values that differ by less than 0.008 from that of the Lyman limit system. The abundance of O with respect to Fe in the Lyman limit system is not much different from the solar abundance ratio. The opacity of the Lyman limit system below 990 Å and the numerous features arising from Galactic H₂ block a moderate fraction of important extragalactic features in the *FUSE* wavelength band. Nevertheless, supplementary spectra at low resolution plus a moderate resolution near-UV spectrum over a limited wavelength range recorded by the Space Telescope Imaging Spectrograph (STIS) on the *Hubble Space Telescope* helped to substantiate our identifications of systems in the *FUSE* spectrum. The low-resolution STIS spectrum also revealed 4 absorption features shortward of the quasar's Ly α emission, which we interpret to arise from additional systems showing only the Ly α feature. Spectroscopy of 7 galaxies with $M_R \lesssim -20$ within approximately 2' of PHL 1811 indicated that 2 of them are near the redshift of the quasar and 4 have redshifts within 850 km s^{-1} of the extragalactic absorption systems. The Lyman limit system is likely associated with an L^* galaxy at $z = 0.0808$ lying $23''$ ($34 h_{70}^{-1} \text{ kpc}$) from the sightline, with absorption arising in the halo of the galaxy or in an unusually large galactic disk. It is also possible that the absorbing material may be tidal debris arising from the galaxy's interactions with a neighbor lying $88 h_{70}^{-1} \text{ kpc}$ from the sightline, or more extensive intragroup or intracluster gas. Finally, in addition to prominent features at very low velocities arising from the disk of our Galaxy, the strong resonance transitions of C II and Mg II show evidence for material at $v \approx -200 \text{ km s}^{-1}$; the column densities of these two species suggest that $17.7 < \log N(\text{H I}) < 18.1$ if the material has a solar composition.

Subject headings: intergalactic medium – galaxies: halos – quasars: absorption lines – quasars: individual (PHL 1811) – ultraviolet: ISM

1. Introduction

In an optical follow-up on the survey of Faint Images of the Radio Sky at Twenty Centimeters (FIRST), Leighly et al. (2001) recognized that PHL 1811 is a quasar with an apparent magnitude at B and R of 13.9 and a redshift $z_{\text{em}} = 0.192$. They stated that “These properties make it the second-brightest quasar (in apparent magnitude) known with $z > 0.1$ after 3C 273.” This extraordinary finding presented an attractive prospect for research on the nature of gas systems at low redshifts, if indeed interesting systems were in front of the quasar and the quasar’s ultraviolet brightness were sufficient to yield a spectrum of good quality in a reasonable observing time. Investigations of this type are important since absorption systems in front of low- z quasars offer the prospect of identifying and characterizing specific galaxies that are likely to be associated with the material. A quick reference for some fundamental attributes of PHL 1811 is given in Table 1. Additional background information and a history of the discovery of this object are given by Leighly et al. (2001).

In order to examine the potential of PHL 1811 for studying intervening absorption systems, we obtained a brief, exploratory exposure using the *Far Ultraviolet Spectroscopic Explorer (FUSE)* (Moos et al. 2000) to record a spectrum from 907 to 1185 Å. However, there is a virtually complete attenuation of the spectrum at wavelengths below the Lyman limit of an absorption system at $z = 0.08092$, discussed in §5.1. This spectrum, presented in §2.1, shows that the quasar’s flux level is sufficient to yield a good spectrum at wavelengths covered by *FUSE* and the *Hubble Space Telescope (HST)*. We also made use of the following *HST* observations at longer wavelengths to help in substantiating systems identified in the *FUSE* spectrum: (1) exposures using the G140L and G230L configurations on the Space Telescope Imaging Spectrograph (STIS) to give low resolution coverages of the wavelength ranges 1150–1700 and 1600–3150 Å (§2.2.1), respectively, and (2) an exposure using the G230MB mode on STIS that covered a small wavelength interval (2760–2910 Å) at moderate resolution (§2.2.2). Next, a more complete understanding of the line of sight to PHL 1811 can arise from a series of observations taken from the ground, where we identify specific foreground galaxies that might be responsible for the absorption systems that appear in the quasar’s ultraviolet spectrum. To find these candidate galaxies, we recorded an image

¹Based on observations from (1) the NASA-CNES-CSA *Far Ultraviolet Spectroscopic Explorer (FUSE)* mission operated by Johns Hopkins University, supported by NASA contract NAS5-32985, (2) the NASA/ESA *Hubble Space Telescope* obtained at the Space Telescope Science Institute, which is operated by the Association of Universities for Research in Astronomy, Inc., under NASA contract NAS 5-26555, and (3) the Apache Point Observatory 3.5 m telescope, which is owned and operated by the Astrophysical Research Consortium.

²Present address: Space Telescope Science Institute, 3700 San Martin Dr., Baltimore, MD 21218

Table 1. Properties of PHL 1811^a

| Property | Value |
|--|--|
| Alternate Name | FIRST J215501–092224 |
| Equatorial Coordinates (J2000.0) α, δ | 21 55 01.48, –09 22 24.7 |
| Galactic Coordinates ℓ, b | 47.47, –44.82 |
| Velocity Conversion ^b | $v_{\text{LSR}} = v_{\odot} + 7.2 \text{ km s}^{-1}$ |
| Foreground Galactic H I (from 21-cm emission) ^c | $4.2 \times 10^{20} \text{ cm}^{-2}$ centered at $v_{\text{LSR}} \approx -3 \text{ km s}^{-1}$ |
| Foreground reddening from our Galaxy $E(B – V)$ | 0.046 |
| Optical Classification | Narrow-line Seyfert 1 Galaxy |
| Power-law exponent α for Optical Continuum Flux $F(\nu)$ | –0.4 |
| Radio flux (20 cm) | 1.4 mJy |
| Apparent Magnitudes ^d | $O = E = 13.9$ |
| Flux 990 – 1400 Å ^e | $5 \times 10^{-14} \text{ erg cm}^{-2} \text{ s}^{-1} \text{ Å}^{-1}$ |
| Flux 2 – 10 keV | $1.6 \times 10^{-13} \text{ erg cm}^{-2} \text{ s}^{-1}$ |
| Emission-line Redshift z_{em} | 0.192 |
| M_V | –25.9 ($H_0 = 70 \text{ km s}^{-1} \text{ Mpc}^{-1}$) |

^aExcept as noted, all information is from Leighly et al. (2001).

^bUsing the standard IAU definition of the conversion from a heliocentric velocity v_{\odot} to a local standard of rest velocity v_{LSR} (Kerr & Lynden-Bell 1986). For the definition given by Mihalas & Binney (1981), replace 7.2 km s^{-1} by 5.7 km s^{-1} .

^c (Hartmann & Burton 1997).

^dMagnitudes from the POSS I plates and USNO-A2.0 catalog (Monet et al. 1996).

^eThis paper – see Figs. 1a–c and 2.

covering a 7.6×7.6 arc-min field surrounding the quasar (§3.1), identified non-stellar objects, and recorded their spectra (§3.2) to obtain the galaxy redshifts (§4.3).

Despite the relatively short exposure time, the *FUSE* spectrum exhibits many interesting absorption features. A large number of lines arise from atoms and H₂ in the disk of our Galaxy. These features often block those originating from redshifted systems, which made the identifications of the latter less certain. Nevertheless, we succeeded in identifying 7 absorption systems (§4.1), and we measured equivalent widths of their unobscured features (§4.2) along with those that arise from the Galaxy. The properties of these low- z systems are discussed in §5, including one that has sufficient neutral hydrogen to create a completely opaque Lyman limit (and high Lyman series) absorption below about 988 Å (§5.1). In addition to the systems identified from the *FUSE* spectrum, we also recognized four additional systems showing only Ly α in the low-resolution STIS spectrum.

Ultimately, our overall understanding of the foreground to PHL 1811 relies on the combination of the absorption-line system identifications with the measurements of galaxy redshifts, and this in turn permits us to express some conclusions on the relationships between the absorbing gases and the outer portions (or neighboring regions) of the galaxies (§6). Finally, we offer some brief comments about the Galactic absorption features, including the normal, low-velocity interstellar gas (§7.1) and a detection of a new high-velocity gas system in the halo of our Galaxy (§7.2).

2. Ultraviolet Observations

2.1. FUSE

FUSE observed PHL 1811 with the light of the quasar centered in the LiF1 LWRS ($30'' \times 30''$) aperture for 11.3 ksec on 22 June 2001, as a part of a guaranteed observing program for the *FUSE* Science Team. The wavelength resolving power of *FUSE* is $R = \lambda/\Delta\lambda \approx 20,000$, which corresponds to 12 detector pixels. The spectra were reduced using Version 1.8.7 of the standard CALFUSE reduction pipeline (Sahnow et al. 2000). The wavelength coverages of different combinations of spectrographs and detectors, known as channels, are listed in Table 2. Data from the LiF1B channel from 1125 to 1152 Å were rejected because they were degraded to an unacceptable level by a partial blockage by a wire mesh in front of the detector (Sahnow et al. 2000). Virtually all of the flux in the wavelength coverage of the SiC1B channel was blanked out by absorption from a Lyman limit system (LLS) in front of the quasar (§5.1). Hence this channel was not used.

Investigators who present *FUSE* data often display separately the spectra recorded by

Table 2. *FUSE* Channels

| Channel Name | λ (Å) | Coverage | $\sigma(F_\lambda)$ (10^{-14} erg cm $^{-2}$ s $^{-1}$ Å $^{-1}$) |
|--------------------|------------------|----------|--|
| SiC1A | 1003–1090 | | 2.25 |
| SiC1B | 907–993 | | ... ^a |
| SiC2A | 918–1005 | | 1.75 |
| SiC2B | 1017–1103 | | 3.0 |
| LiF1A | 987–1083 | | 1.2 |
| LiF1B ^b | 1095–1125 | | 1.25 |
| | 1152–1185 | | 1.7 |
| LiF2A | 1087–1180 | | 1.25 |
| LiF2B | 987–1075 | | 1.55 |

^aThis channel was not used; see text.

^bThe spectrum from this channel was interrupted by a segment of poor quality from 1125 to 1152Å.

the different channels. The reasons for doing so are twofold: first, separate plots of the individual outputs allow one to identify spurious features arising from localized, extraordinarily large deviations in the detector sensitivity (that are not properly corrected in the data reduction) and, second, the channels have slightly different resolutions and wavelength zero points. While we recognized the advantages for separate depictions of the spectra, we were nevertheless driven to display a composite spectrum of PHL 1811 from all of the channels in order to show information with an acceptable signal-to-noise ratio. Otherwise, many of the weakest absorption features would have been extremely difficult to identify. Significant spectral features that could be seen in one channel but were conspicuously absent in others were recognized as probably spurious and rejected. Only three such features can be easily seen in the composite spectrum, and they are marked with \times 's in Figure 1. They appear at 999.8, 1140.8 and 1152.1 Å.

The spectra were combined in two ways for two different applications. One composite spectrum was created to give the best looking plot for displaying and identifying the features, while another was derived slightly differently to preserve the integrity of the estimated errors for measuring the equivalent widths of lines. In both cases, small shifts (up to 5 pixels ≈ 0.1 Å) to compensate for differences in the wavelength zero points were implemented before the spectra were combined. For the spectrum that appears in Fig. 1, the most exact (noninteger) shifts were implemented to give the best possible resolution. Also, for display purposes, a convolution with a Gaussian of width 2.5 pixels (FWHM) was implemented. The spectrum created for equivalent width measurements had no such convolution performed, and the shifts between spectra were restricted to integer values to avoid the need for mid-pixel interpolations, which would alter the noise in unpredictable ways. In all instances, channel spectra were combined with weights proportional to their respective inverse variances. Estimates of these variances were based on the total event counts as a function of position, but only after they were smoothed with a 45-pixel wide kernel (≈ 0.9 Å) so that we could avoid biasing the outcomes by small-scale intensity shifts arising from either noise or real absorption features. Near the ends of individual spectra, the weight factors gradually tapered (over 50 pixels) to zero to avoid abrupt changes in the composite spectrum at the end of any channel's coverage. One may derive an approximate value for the expected error in each pixel (of the combined spectrum) from the expression $(\sum \sigma(F_\lambda)^{-2})^{-1/2}$, where representative values of the flux errors $\sigma(F_\lambda)$ are listed in Table 2 (to obtain the noise per resolution element, divide by $12^{1/2}$). Differences in the channel coverages result in moderate changes in this error of the composite fluxes from one wavelength to the next. For instance, the interval from 1083 to 1087 Å has a poor signal-to-noise ratio, compared to the rest of the spectrum, because it is covered only by the SiC1A and SiC2B channels that have lower sensitivities than the LiF channels at long wavelengths.

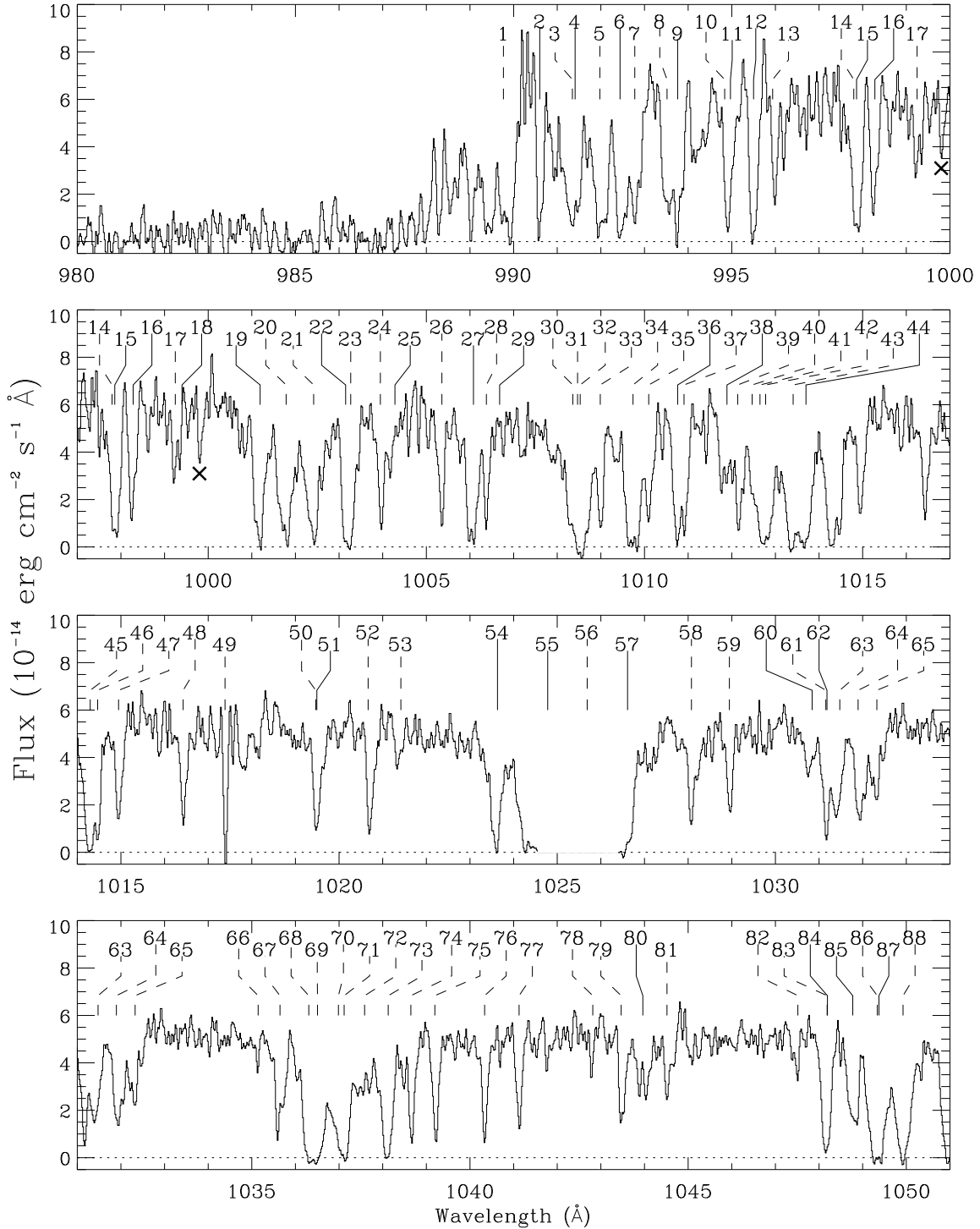


Fig. 1a.— Spectrum of PHL 1811 recorded by *FUSE*. Numbers and lines (dashed: Galactic features, solid: extragalactic features) identify features listed in Tables 3 and 4. The vicinity of the geocoronal Ly β emission feature in the core of the Galactic absorption is omitted, but second order diffraction of the He I λ 584.3 emission line can be seen at 1168.7 \AA . Features created by uncorrected detector artifacts are labeled with an “ \times ”.

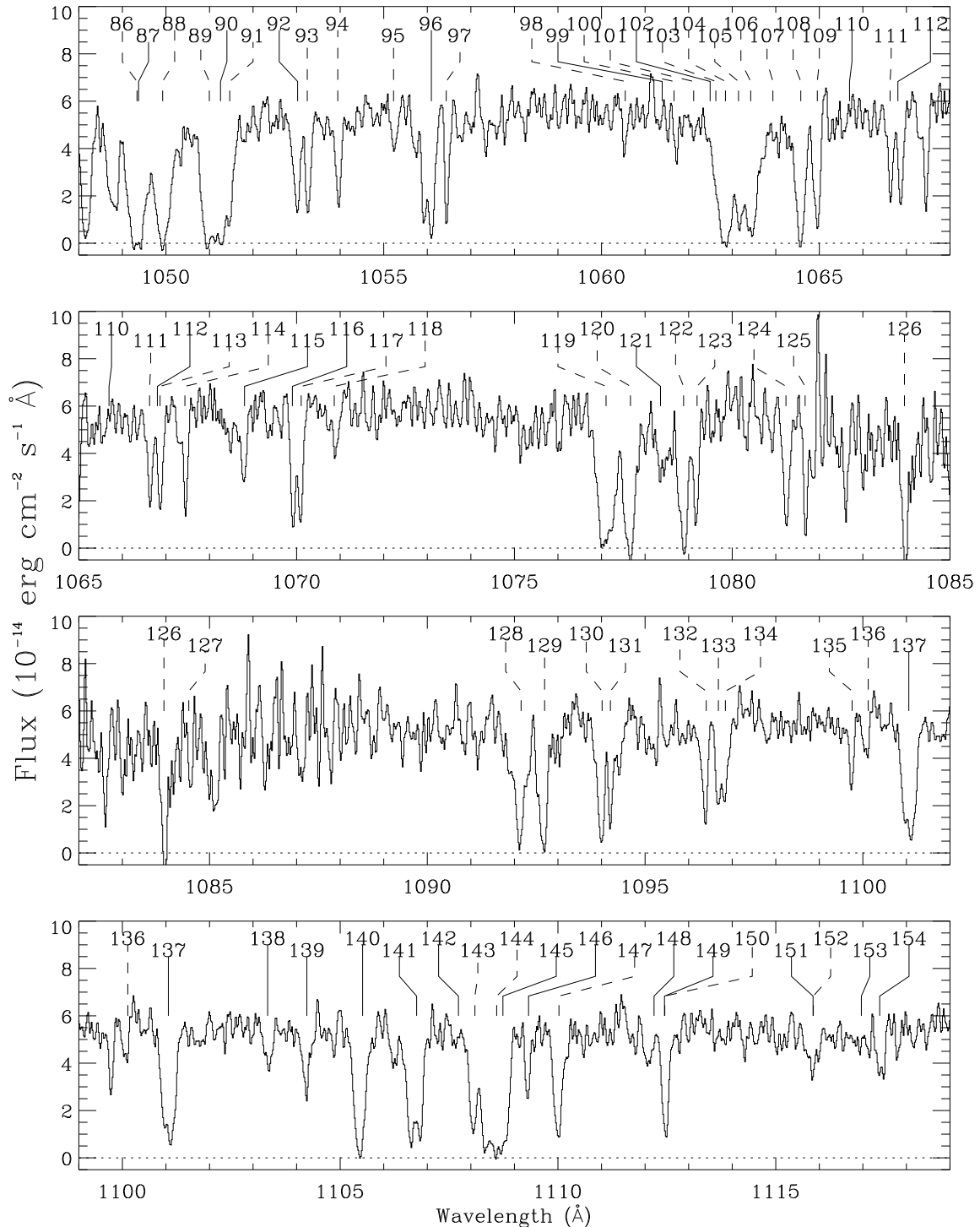


Fig. 1b.— continued

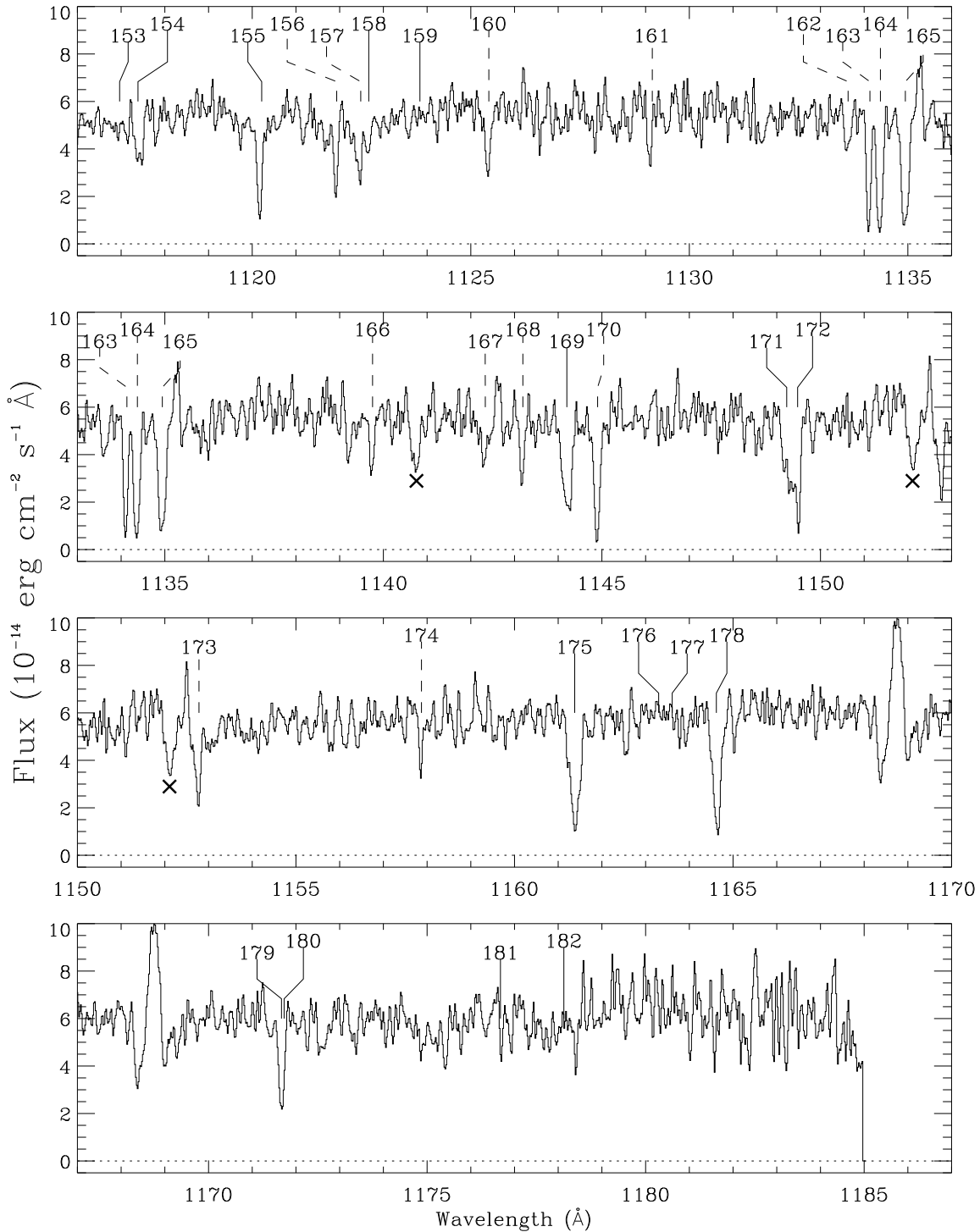


Fig. 1c.— continued

Currently, without any special adjustments the heliocentric wavelength scale for the LiF1A *FUSE* spectrum, our most reliable channel for wavelengths, can have errors that correspond to offsets in radial velocity as large as 15 km s^{-1} , and these errors change slightly with wavelength. In order to refine the wavelengths, we applied an overall shift such that the Galactic absorption features, marked by dashed lines³ in Fig. 1, agreed with our best expectation for their heliocentric velocity $v_\odot \approx -10 \text{ km s}^{-1}$, based on the centroid of the H I 21-cm emission observed in the Leiden–Dwingeloo Survey very near the direction of PHL 1811 (Hartmann & Burton 1997) – see Table 1. After revising the wavelength scale, we find that Galactic features that have $W_\lambda > 50 \text{ m}\text{\AA}$ and no plausible interference from other lines (shown with endnote *b* in Table 3) have an average v_\odot equal to -9.7 km s^{-1} with an rms dispersion of 5.4 km s^{-1} – see the third column of Table 3. The correspondence in velocity between the absorption features in PHL 1811 and the 21-cm emission may not be exact, since the 21-cm telescope beam samples many directions somewhat offset from the line of sight to the quasar.

2.2. STIS

2.2.1. G140L and G230L Spectra

To help in confirming the reality of our identifications of systems in the *FUSE* spectrum and find systems that appear only at Ly α , we made use of low-resolution spectra recorded by the Space Telescope Imaging Spectrograph (STIS) for a program intended for a study of the properties of PHL 1811 (program nr. 9181). The spectra were recorded on 12 December 2001, using the G140L ($R \approx 1000$) and G230L ($R \approx 500$) gratings and the $0''.2$ entrance slit. To reduce the effects of any fixed pattern noise for this bright target, four subexposures were obtained with the target stepped along the slit. We applied the standard pipeline processing (CALSTIS Version 2.11) and then summed and resampled the spectra to yield exposures of 6640 and 1667 s for the G140L and G230L modes, respectively. The combined spectra with our proposed identifications (§4.1) are presented in Figures 2 and 3. For the G140L spectrum, we achieved $S/N = 100$ (per resolution element), while for the G230L $S/N = 90$.

Systematic errors in the wavelength scale for STIS low resolution spectra range from 0.5 to 1.0 pixels (Leitherer 2001), which corresponds to $0.25 - 0.5 \text{ \AA}$ and $0.75 - 1.5 \text{ \AA}$ for the G140L and G230L modes, respectively.

³The markers uniformly point to wavelengths corresponding to $v_\odot = -10 \text{ km s}^{-1}$.

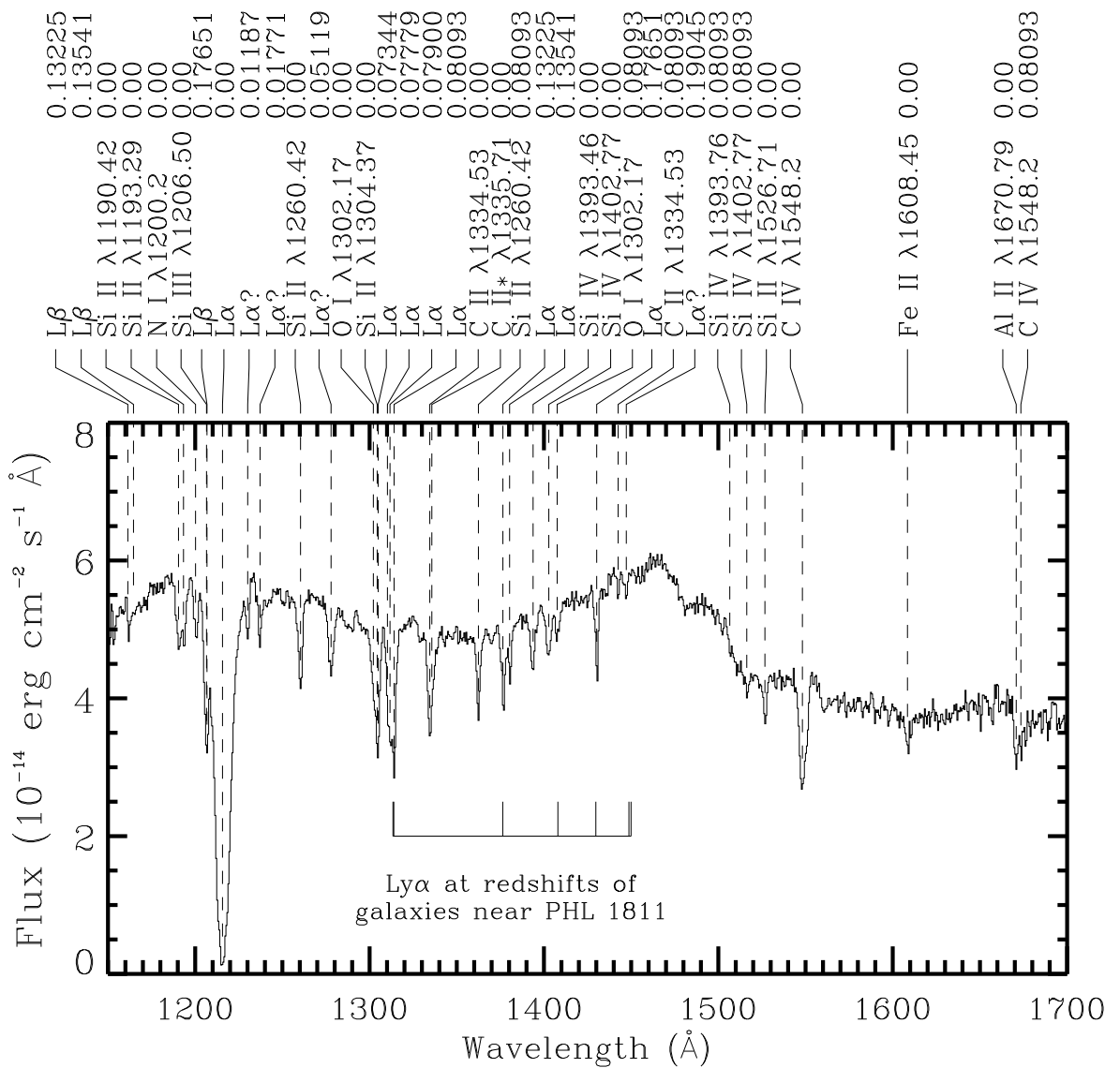


Fig. 2.— Spectrum of PHL 1811 recorded by STIS in the G140L mode. The double-peaked, broad emission centered on 1480 Å represents the Ly α + N V features of the quasar. Identifications of the absorption lines and their laboratory wavelengths are shown above the panel, followed by the redshifts in each case. The expected positions of Ly α features at the redshifts of galaxies discussed in §4.3 are indicated by short vertical lines below the spectrum. Galactic absorption by Ly α is the very strong feature; transitions of Si III λ 1206.5, O I λ 1302.2, and Si II λ 1304.4 should also be prominent. At the resolution of this spectrum these features interfere with the extragalactic features at nearly the same wavelengths. Ly α identifications with question marks denote features from systems that are visible only at Ly α ; these provisional assignments are not confirmed by other features elsewhere in either the FUSE or STIS spectra.

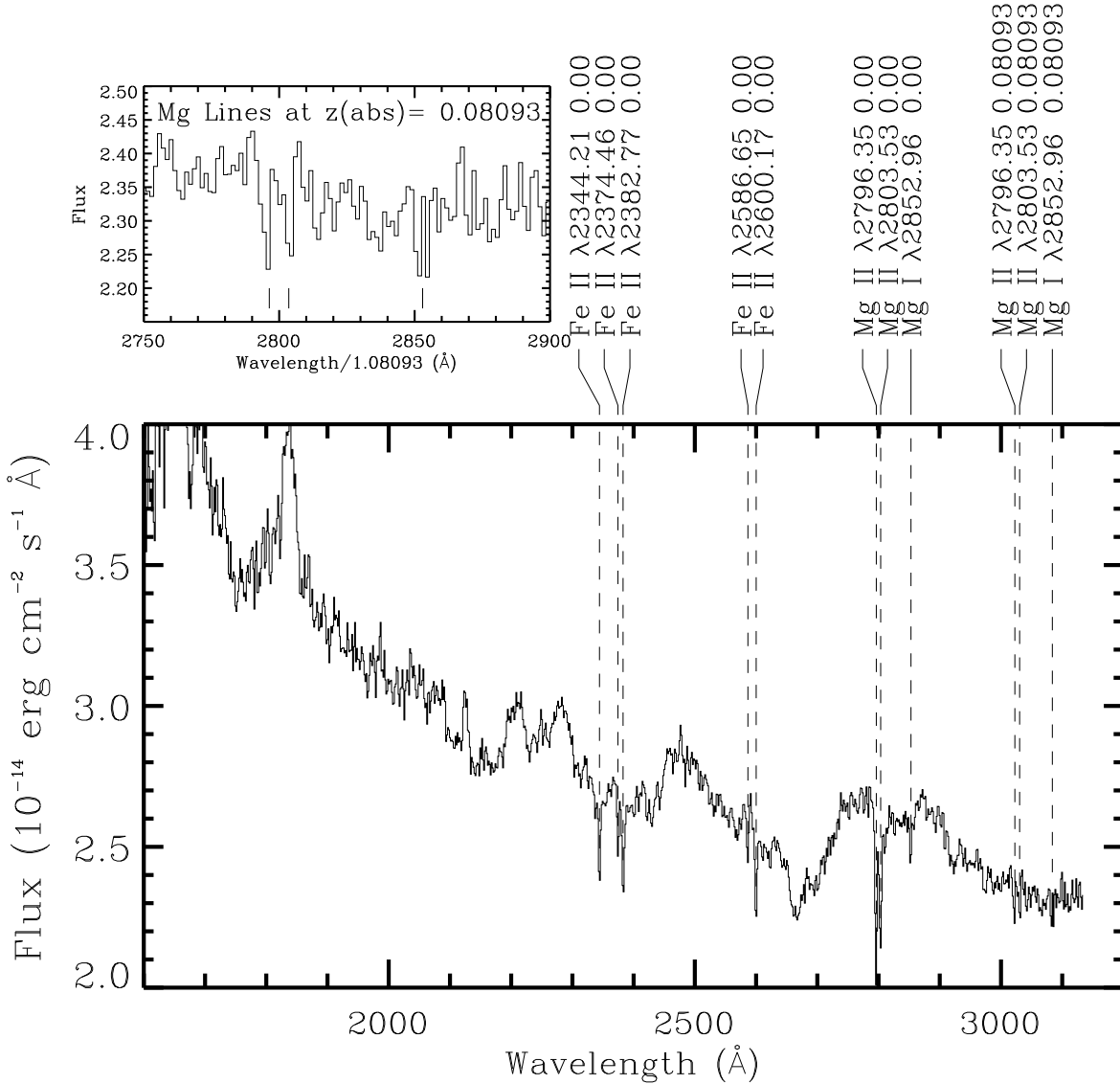


Fig. 3.— Spectrum of PHL 1811 recorded by STIS in the G230L mode with line identifications. The small panel above the main spectrum shows a magnified view of the region covering one Mg I (right-hand feature) and two Mg II absorption lines (remaining two features) in the Lyman limit system at $z = 0.08093$, with wavelengths converted to the system's rest frame. The emission feature at 1846 Å is from the C IV $\lambda 1549$ doublet, and the apparent absorption at 2680 Å (2248 Å in the quasar's rest frame) is a gap between pseudo-continua created by emission-line complexes of Fe II.

2.2.2. G230MB Spectrum

We obtained a moderate resolution ($R \approx 6000$) STIS G230MB spectrum of PHL 1811 in the vicinity of the Mg II 2800 Å doublet from observations taken on 22 October 2001 as part of an *Hubble Space Telescope (HST)* snapshot (SNAP) observing program designed to search for weak Mg II absorption from High Velocity Clouds near the Milky Way toward AGNs that are bright in the ultraviolet (Program 9128). For this program, PHL 1811 was observed for a total of 1200 s, with two sub-exposures taken for cosmic ray rejection (CR-SPLIT=2), using the $52'' \times 0''.2$ slit and G230MB grating centered at 2836 Å (covering 2758–2914 Å). The object was placed in the E1 pseudo-aperture for improved charge transfer efficiency, and the CCD gain was set to $1\text{e}^-/\text{ADU}$. STIS spectra recorded with the CCD benefit from a customized extraction more than the STIS spectra discussed in §2.2.1, which were obtained with the MAMA detectors. For instance, to preserve the LSF sampling and improve cosmic ray rejection, we refrained from binning the signals along either axis. We used the standard pipeline CALSTIS reduction to correct the bias (using the overscan and bias image), subtract the flat field and dark current, and combine the sub-exposures for cosmic ray rejection. We extracted a spectrum from the wavelength-calibrated, geometrically-corrected, two-dimensional image using tasks in the IRAF⁴ *twodspec/apextract* package. A reference spectrum created by the coaddition of 15 separate targets from the same SNAP program was used to define the center of the aperture as a function of wavelength, and the final spectrum was then extracted using variance weighting. As expected, the resulting one-dimensional spectrum (Fig. 4) shows fewer artifacts and a somewhat improved quality ($S/N = 18$ per resolution element) when compared to the pipeline extraction, but all of the identified features were detectable in both extractions.

3. Ground-Based Observations

3.1. Image of the Field Surrounding PHL 1811

Eight 120 s *R*-band images of the field of PHL 1811 covering a $7''.6 \times 7''.6$ field of view were taken at the MDM 1.3-m McGraw-Hill Telescope on 29 June 2001. The seeing was $1''.2$. A portion of the combined *R*-band image is presented in Figure 5. Standard stars in the field of PG 1633+099 (Landolt 1992) were used to calibrate the magnitude of PHL 1811.

⁴IRAF is distributed by the National Optical Astronomy Observatories, which are operated by the Association of Universities for Research in Astronomy, Inc., under cooperative agreement with the National Science Foundation.

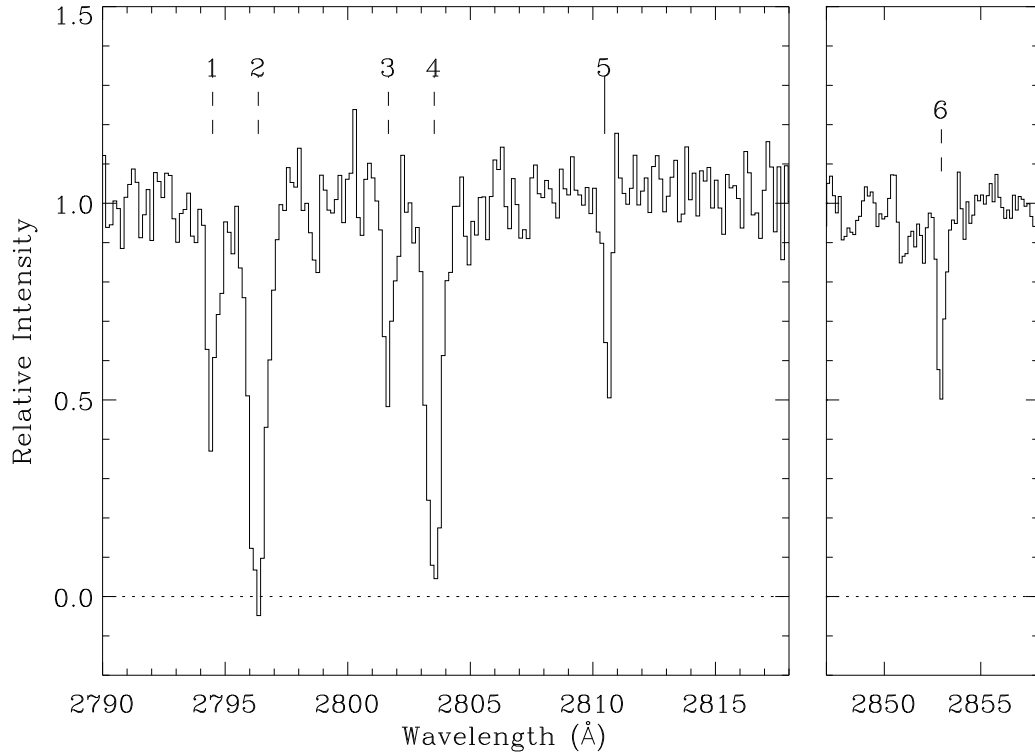


Fig. 4.— A section of the G230MB spectrum covering noteworthy features arising from the disk of the Galaxy, the high velocity cloud in the Galactic halo, and the Lyman limit absorption system at $z_{\text{abs}} = 0.08093$. Identifications and equivalent widths of the features are given in Table 6. As in Fig. 1, solid lines mark Galactic features and dashed ones mark extragalactic ones. While the feature at 2798.6 \AA with $W_{\lambda} \approx 60 \text{ m\AA}$ appears to be real, we were unable to find a plausible identification.

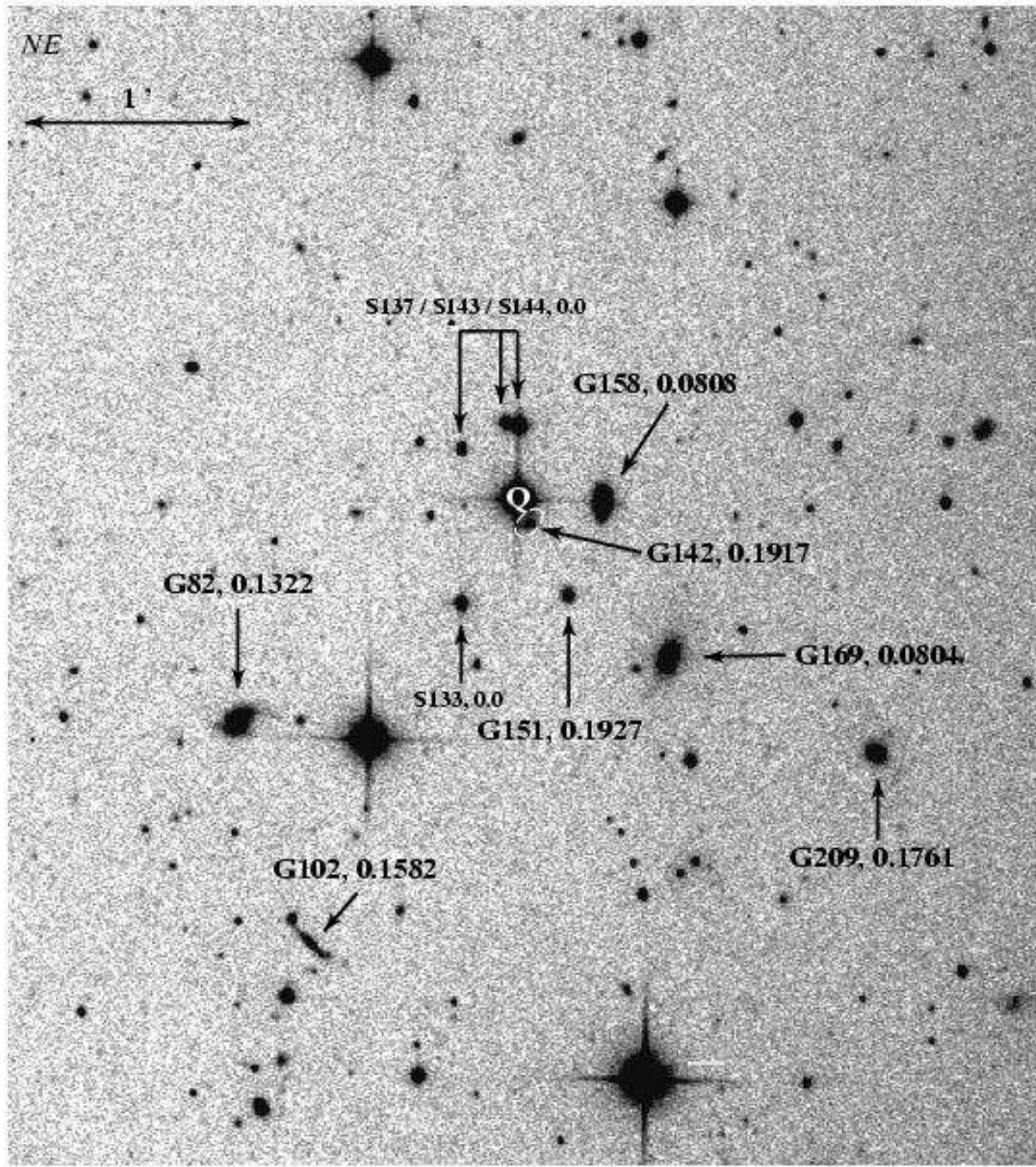


Fig. 5.— Portion of a 16 min *R*-band image of the field of PHL 1811 (marked with a “Q”) taken at the MDM 1.3-m McGraw-Hill Telescope. Galaxies (G) and stars (S) for which redshifts were obtained at the APO 3.5 m Telescope (and which are listed in Table 7) are marked, along with their redshifts.

Light cirrus was present at dawn, suggesting that conditions may have not been photometric, but our value of $R = 14.1$ for the QSO is consistent with the value of 13.9 measured from POSS-I E plates and listed in the USNO-A2.0 catalog (Monet et al. 1996). To determine accurate coordinates of all the objects in the field, we identified stars which could be seen both in the CCD image and in the “First-generation” SERC-J STScI Digitized Sky Survey⁵ image. Since precise coordinates of stars can be measured from the latter data, we were able to construct a plate-solution for the CCD image, giving positions of all objects accurate to $\simeq \pm 1$ arcsec. To catalog objects detected in the image, and to derive their magnitudes, we used the software package **sextractor** (Bertin & Arnouts 1996). Approximately 300 objects were identified down to a magnitude limit of $R = 21.5$.

3.2. Galaxy Spectra

In order to identify probable sources of the absorption systems detected in the FUSE and STIS data (particularly the LLS at $z = 0.08093$) we proceeded to obtain redshifts of objects in the field of PHL 1811. Spectra of eleven candidates were recorded using the Apache Point Observatory (APO) 3.5 m Telescope⁶. To check for compact galaxies near the sight line, spectra were obtained for several objects classified as stars, as well as for the obvious bright galaxies. Data were taken on 17, 18, and 20 November 2001 using the Double Imaging Spectrograph (DIS) and low resolution gratings. Spectra were obtained in long-slit mode, with total exposure times ranging from 1200 to 3500 seconds per object, and processed in the conventional manner. The data were wavelength calibrated using helium-neon-argon arc-lamp exposures, which were taken throughout the night. The spectra covered a wavelength range of 3900–5500 Å in the blue and 5500–10,000 Å in the red. The final resolution of the spectra was $\simeq 9.0$ Å and 14.0 Å FWHM for the blue and red channels of the spectrograph, respectively.

⁵Based on photographic data obtained using the UK Schmidt Telescope. The UK Schmidt Telescope was operated by the Royal Observatory, Edinburgh, with funding from the UK Science and Engineering Research Council, until 1988 June, and thereafter by the Anglo-Australian Observatory. The Digitized Sky Survey was produced at the Space Telescope Science Institute under a US Government grant NAG W-2166.

⁶The APO 3.5 m Telescope is owned and operated by the Astrophysical Research Consortium.

4. Measurements

4.1. Identifications of Absorbing Systems

The *FUSE* spectrum was used as the primary source of information for recognizing absorption systems, since it covered a large number of features with a satisfactory wavelength resolving power. The three much lower resolution STIS spectra helped to confirm most of the absorption systems and provide some additional information. Prior to our attempts to pick out features from extragalactic systems, we identified obvious features arising from our Galaxy. In the *FUSE* spectrum, features from Galactic H₂ are especially plentiful. On many occasions the foreground picket fence created by these features interfered with important extragalactic lines that could have corroborated tentative identifications of lines seen at other locations.

The easiest redshifted system to recognize is one that shows Lyman limit absorption that begins at about 988 Å and completely blocks light from the quasar at shorter wavelengths. As one might expect, of all the extragalactic systems we identified, this one shows the most features in the *FUSE* spectrum. Six other, much weaker absorption systems in front of PHL 1811 were also identified, three of which have redshifts that differ by less than 2500 km s^{−1} from that of the Lyman limit system (LLS) at $z_{\text{abs}} = 0.08093$.

The Galactic lines appearing in the *FUSE* spectrum are listed in Table 3, along with their measured radial velocities and equivalent widths. Features belonging to the extragalactic systems are listed in Table 4. The redshifts listed in the first column of Table 4 are designated on the basis of where the most prominent lines are seen on the *FUSE* wavelength scale. They are uncertain by about ± 0.00003 because the *FUSE* wavelengths can have residual errors even after they are calibrated by the positions of the Galactic features, as described in §2.1. The observed wavelengths listed in the second column of Table 4 are simply computed from the laboratory wavelengths using these redshifts (except for line nr. 151 – see endnote *d* of the table); they do not represent actual measurements of the positions of individual features. The last columns of Tables 3 and 4 show the identification numbers that are used in Fig. 1 to mark the respective lines.

Table 3. *FUSE* Observations of Galactic Lines

| Transition Rest λ (Å) | Species Ident. | v_{\odot} (km s $^{-1}$) | $W_{\lambda} \pm 1\sigma$ error (mÅ) | nr. ^a |
|----------------------------------|--------------------------------|--------------------------------|---|------------------|
| 989.80/87 | N III/Si II | ... | ... | 1 |
| 991.38 | H ₂ L 9–0 R(0) | ... | ... | 3 |
| 992.01 | H ₂ L 9–0 R(1) | ... | ... | 5 |
| 992.81 | H ₂ L 9–0 P(1) | ... | ... | 7 |
| 993.55 | H ₂ L 9–0 R(2) | ... | ... | 8 |
| 994.87 | H ₂ L 9–0 P(2) | ... | ... | 10 |
| 995.97 | H ₂ L 9–0 R(3) | 6.4 | 102±21 | 13 |
| 997.83 | H ₂ L 9–0 P(3) | ... | ... | 14 |
| 999.28 | H ₂ L 9–0 R(4) | ... | ... | 17 |
| 1001.82 | H ₂ L 8–0 R(0) | ... | 282±44 ^b | 20 |
| 1002.45 | H ₂ L 8–0 R(1) | -5.4 | 303±38 | 21 |
| 1003.30 | H ₂ L 8–0 P(1) | ... | ... | 23 |
| 1003.98 | H ₂ L 8–0 R(2) | ... | 117±21 ^b | 24 |
| 1005.39 | H ₂ L 8–0 P(2) | -10.3 | 111±20 | 26 |
| 1006.41 | H ₂ L 8–0 R(3) | -10.4 | 108±21 | 28 |
| 1008.39 | H ₂ L 8–0 P(3) | ... | ... | 30 |
| 1008.50/55 | H ₂ W 0–0 R(1)/R(0) | ... | ... | 31 |
| 1008.56 | H ₂ W 0–0 R(0) | ... | ... | 32 |
| 1009.02 | H ₂ W 0–0 R(2) | -9.4 | 115±22 | 33 |
| 1009.77 | H ₂ W 0–0 Q(1) | ... | ... | 34 |
| 1010.13 | H ₂ W 0–0 R(3) | ... | ... | 35 |
| 1010.94 | H ₂ W 0–0 Q(2) | ... | ... | 37 |
| 1012.17 | H ₂ W 0–0 P(2) | ... | ... | 39 |
| 1012.50 | S III | ... | ... | 40 |
| 1012.68 | H ₂ W 0–0 Q(3) | ... | ... | 41 |
| 1012.81 | H ₂ L 7–0 R(0) | ... | ... | 42 |
| 1013.44 | H ₂ L 7–0 R(1) | ... | ... | 43 |
| 1014.33 | H ₂ L 7–0 P(1) | ... | ... | 45 |
| 1014.50 | H ₂ W 0–0 P(3) | ... | ... | 46 |
| 1014.98 | H ₂ L 7–0 R(2) | -8.8 | 101±25 | 47 |

Table 3—Continued

| Transition Rest λ (Å) | Species Ident. | v_{\odot} (km s $^{-1}$) | $W_{\lambda} \pm 1\sigma$ error (mÅ) | nr. ^a |
|----------------------------------|---------------------------|--------------------------------|---|------------------|
| 1016.46 | H ₂ L 7–0 P(2) | −7.6 | 115±17 | 48 |
| 1017.42 | H ₂ L 7–0 R(3) | −6.0 | 133±17 | 49 |
| 1019.50 | H ₂ L 7–0 P(3) | ... | ... | 50 |
| 1020.70 | Si II | 2.3 | 149±17 | 52 |
| 1021.45 | HD L 7–0 R(0) | ... | 41±17 | 53 |
| 1025.72 | H I (Ly β) | ... | ... | 56 |
| 1028.11 | H ₂ L 6–0 P(2) | −10.5 | 122±15 | 58 |
| 1028.98 | H ₂ L 6–0 R(3) | −6.6 | 95±15 | 59 |
| 1031.19 | H ₂ L 6–0 P(3) | ... | ... | 61 |
| 1031.51 | Cl I | ... | ... | 63 |
| 1031.93 | O VI | ... | 337±26 ^{b,c} | 64 |
| 1032.36 | H ₂ L 6–0 R(4) | ... | ... | 65 |
| 1035.18 | H ₂ L 6–0 P(4) | ... | 23±11 | 66 |
| 1036.34 | C II ^d | −200 | 137±22 | 67 |
| 1036.34 | C II | ... | ... | 68 |
| 1036.54 | H ₂ L 5–0 R(0) | ... | ... | 69 |
| 1037.02 | C II* | ... | ... | 70 |
| 1037.15 | H ₂ L 5–0 R(1) | ... | ... | 71 |
| 1037.62 | O VI | ... | ... | 72 |
| 1038.16 | H ₂ L 5–0 P(1) | −15.7 | 255±25 | 73 |
| 1038.68 | H ₂ L 5–0 R(2) | −4.5 | 126±19 | 74 |
| 1039.23 | O I | −4.4 | 132±17 ^e | 75 |
| 1040.37 | H ₂ L 5–0 P(2) | −8.0 | 120±14 | 76 |
| 1041.16 | H ₂ L 5–0 R(3) | −9.9 | 104±14 | 77 |
| 1042.85 | HD L 5–0 R(0) | ... | 14±15 | 78 |
| 1043.50 | H ₂ L 5–0 P(3) | −3.5 | 105±14 | 79 |
| 1044.55 | H ₂ L 5–0 R(4) | −9.4 | 81±15 | 81 |
| 1047.55 | H ₂ L 5–0 P(4) | ... | 31±12 | 82 |
| 1048.22 | Ar I | −15.7 | 226±19 | 83 |
| 1049.37 | H ₂ L 4–0 R(0) | ... | ... | 86 |

Table 3—Continued

| Transition Rest λ (Å) | Species Ident. | v_{\odot} (km s $^{-1}$) | $W_{\lambda} \pm 1\sigma$ error (mÅ) | nr. ^a |
|----------------------------------|---------------------------------|--------------------------------|---|------------------|
| 1049.96 | H ₂ L 4–0 R(1) | ... | ... | 88 |
| 1051.03 | H ₂ L 4–0 P(1) | ... | ... | 89 |
| 1051.50 | H ₂ L 4–0 R(2) | ... | ... | 91 |
| 1053.28 | H ₂ L 4–0 P(2) | -4.8 | 115±14 | 93 |
| 1053.98 | H ₂ L 4–0 R(3) | -6.0 | 99±15 | 94 |
| 1055.26 | Fe II | ... | 27±18 | 95 |
| 1056.47 | H ₂ L 4–0 P(3) | -6.7 | 88±14 | 97 |
| 1060.58 | H ₂ L 4–0 P(4) | ... | 31±14 | 98 |
| 1061.70 | H ₂ L 4–0 R(5) | ... | 26±15 | 100 |
| 1062.15 | Fe II | ... | 1±20 | 101 |
| 1062.66 | S IV | ... | ... | 103 |
| 1062.88 | H ₂ L 3–0 R(0) | ... | ... | 104 |
| 1063.18 | Fe II | ... | ... | 105 |
| 1063.46 | H ₂ L 3–0 R(1) | ... | ... | 106 |
| 1063.97 | Fe II | ... | 18±20 | 107 |
| 1064.61 | H ₂ L 3–0 P(1) | -10.7 | 237±18 | 108 |
| 1064.99 | H ₂ L 3–0 R(2) | -11.6 | 146±16 | 109 |
| 1066.66 | Ar I | -4.9 | 92±16 | 111 |
| 1066.90 | H ₂ L 3–0 P(2) | -8.5 | 105±17 | 113 |
| 1067.47 | H ₂ L 3–0 R(3) | -4.7 | 93±17 | 114 |
| 1070.14 | H ₂ L 3–0 P(3) | ... | ... | 117 |
| 1070.90 | H ₂ L 3–0 R(4) | ... | 44±14 | 118 |
| 1077.14 | H ₂ L 2–0 R(0) | -7.9 | 408±31 | 119 |
| 1077.70 | H ₂ L 2–0 R(1) | -11.2 | 306±26 | 120 |
| 1078.92 | H ₂ L 2–0 P(1) | -6.7 | 229±22 | 122 |
| 1079.23 | H ₂ L 2–0 R(2) | -16.6 | 100±16 | 123 |
| 1081.27 | H ₂ L 2–0 P(2) | -6.7 | 132±27 | 124 |
| 1081.71 | H ₂ L 2–0 R(3) | -6.1 | 111±33 | 125 |
| 1083.99 | N II | -5.4 | 170±39 | 126 |
| 1084.56/58 | H ₂ L 2–0 P(3)/N II* | ... | ... | 127 |

Table 3—Continued

| Transition Rest λ (Å) | Species Ident. | v_\odot (km s $^{-1}$) | $W_\lambda \pm 1\sigma$ error (mÅ) | nr. ^a |
|----------------------------------|--------------------------------|------------------------------|---------------------------------------|------------------|
| 1092.19 | H ₂ L 1–0 R(0) | −18.6 | 282±25 | 128 |
| 1092.73 | H ₂ L 1–0 R(1) | −18.7 | 217±19 | 129 |
| 1094.05 | H ₂ L 1–0 P(1) | ... | 173±22 ^b | 130 |
| 1094.24 | H ₂ L 1–0 R(2) | ... | 97±18 ^b | 131 |
| 1096.44 | H ₂ L 1–0 P(2) | −16.9 | 114±13 | 132 |
| 1096.72 | H ₂ L 1–0 R(3) | ... | ... | 133 |
| 1096.88 | Fe II | ... | ... | 134 |
| 1099.79 | H ₂ L 1–0 P(3) | −13.9 | 63±11 | 135 |
| 1100.16 | H ₂ L 1–0 R(4) | ... | 35±11 | 136 |
| 1108.13 | H ₂ L 0–0 R(0) | ... | ... | 143 |
| 1108.63 | H ₂ L 0–0 R(1) | ... | ... | 144 |
| 1110.06/12 | H ₂ L 0–0 P(1)/R(2) | ... | 184±15 | 147 |
| 1112.49/58 | H ₂ L 0–0 P(2)/R(3) | ... | ... | 150 |
| 1115.90 | H ₂ L 0–0 P(3) | ... | ... | |
| 1121.97 | Fe II | −15.7 | 56±15 | 156 |
| 1122.52 | Fe III | ... | 64±13 ^b | 157 |
| 1125.45 | Fe II | −15.9 | 54±15 | 160 |
| 1129.19 | C I | ... | 35±16 | 161 |
| 1133.67 | Fe II | ... | 32±13 | 162 |
| 1134.17 | N I | −16.9 | 102±12 ^e | 163 |
| 1134.41 | N I | −14.4 | 144±14 ^e | 164 |
| 1134.98 | N I | −11.8 | 160±14 ^e | 165 |
| 1139.79 | C I | −14.1 | 50±14 | 166 |
| 1142.37 | Fe II | −16.9 | 50±16 | 167 |
| 1143.23 | Fe II | −14.5 | 56±15 | 168 |
| 1144.94 | Fe II | −13.4 | 134±15 | 170 |
| 1152.82 | P II | −17.0 | 85±13 | 173 |
| 1157.91 | C I | ... | 29±11 | 174 |

Table 3—Continued

| Transition Rest λ (Å) | Species Ident. | v_\odot (km s $^{-1}$) | $W_\lambda \pm 1\sigma$ error (mÅ) | nr. ^a |
|----------------------------------|-------------------|------------------------------|---------------------------------------|------------------|
| | | | | |

^aLine identification numbers appearing in Fig. 1. The markers are shifted by -10 km s $^{-1}$ relative to the wavelengths given in the first column.

^bSlight blending with a nearby feature may lead to additional error in W_λ .

^cExistence of O VI is not certain, since a feature is not seen at 1037.62 Å. However C II* and H₂ features near the weaker O VI line make this apparent absence inconclusive.

^dHigh-velocity component – see §7.2.

^ePossible contamination from geocoronal emission may partly fill in this line. For this reason, the real value of W_λ could be larger.

^fThe feature seen at the position of this line is unlikely to arise from H₂ in the Galaxy. The measured equivalent width of 78 ± 16 mÅ for line nr. 151 attributed to extragalactic O VI in Table 4 is comparable to, or slightly greater than, the value of 63 ± 11 mÅ measured for the Lyman 1–0 P(3) line at 1099.79 Å (line nr. 135), a transition whose strength is greater by a factor of 3.3 (Abgrall & Roueff 1989).

Table 4. *FUSE* Observations of Extragalactic Lines

| z_{abs} | Observed λ (Å) | Transition λ (Å) | Species Ident. | $W_r \pm 1\sigma$ error (mÅ) | nr. ^a | |
|------------------|---------------------------|-----------------------------|----------------------|---------------------------------|------------------|----|
| 0.07344 | 1006.67 | 937.80 | H I (Ly ϵ) | -6 ± 23 | 29 | |
| | 1019.49 | 949.74 | H I (Ly δ) | ... | 51 | |
| | 1044.18 | 972.54 | H I (Ly γ) | 127 ± 18 | 80 | |
| | 1048.77 | 977.02 | C III | 190 ± 14 | 85 | |
| | 1061.39 | 988.77 | O I | -5 ± 17 | 99 | |
| | 1062.49 | 989.80/87 | N III/Si II | ... | 102 | |
| | 1101.05 | 1025.72 | H I (Ly β) | 271 ± 15 | 137 | |
| | 1107.71 | 1031.93 | O VI | 23 ± 14 | 142 | |
| | 1112.45 | 1036.34 | C II | ... | 149 | |
| | 1163.60 | 1083.99 | N II | 0 ± 16 | 177 | |
| | 0.07779 | 994.96 | 923.15 | H I (Ly θ) | ... | 11 |
| | | 998.28 | 926.23 | H I (Ly η) | ... | 16 |
| | | 1003.15 | 930.75 | H I (Ly ζ) | ... | 22 |
| | | 1010.75 | 937.80 | H I (Ly ϵ) | ... | 36 |
| | | 1023.62 | 949.74 | H I (Ly δ) | 283 ± 41 | 54 |
| 0.07900 | 1048.19 | 972.54 | H I (Ly γ) | ... | 84 | |
| | 1053.02 | 977.02 | C III | 104 ± 13 | 92 | |
| | 1065.69 | 988.77 | O I | -2 ± 21 | 110 | |
| | 1066.80 | 989.80/87 | N III/Si II | ... | 112 | |
| | 1105.51 | 1025.72 | H I (Ly β) | 260 ± 14 | 140 | |
| | 1112.20 | 1031.93 | O VI | 51 ± 16^b | 148 | |
| | 1116.96 | 1036.34 | C II | 28 ± 18 | 153 | |
| | 999.40 | 926.23 | H I (Ly η) | ... | 18 | |
| | 1004.28 | 930.75 | H I (Ly ζ) | ... | 25 | |
| | 1011.89 | 937.80 | H I (Ly ϵ) | ... | 38 | |
| 0.08093 | 1024.77 | 949.74 | H I (Ly δ) | ... | 55 | |
| | 1049.37 | 972.54 | H I (Ly γ) | ... | 87 | |
| | 1106.75 | 1025.72 | H I (Ly β) | 286 ± 15 | 141 | |
| | 990.60 | 916.43 | H I (Ly ν) | 148 ± 22 | 2 | |
| | 991.41 | 917.18 | H I (Ly μ) | ... | 4 | |

Table 4—Continued

| z_{abs} | Observed λ (Å) | Transition λ (Å) | Species Ident. | $W_r \pm 1\sigma$ error (mÅ) | nr. ^a |
|------------------|---------------------------|-----------------------------|----------------------|---------------------------------|------------------|
| | 992.43 | 918.13 | H I (Ly λ) | ... | 6 |
| | 993.75 | 919.35 | H I (Ly κ) | ... | 9 |
| | 995.49 | 920.96 | H I (Ly ι) | 186±21 | 12 |
| | 997.86 | 923.15 | H I (Ly θ) | ... | 15 |
| | 1001.19 | 926.23 | H I (Ly η) | 258±21 | 19 |
| | 1006.08 | 930.75 | H I (Ly ζ) | 245±20 | 27 |
| | 1013.70 | 937.80 | H I (Ly ϵ) | ... | 44 |
| | 1026.60 | 949.74 | H I (Ly δ) | ... | 57 |
| | 1030.83 | 953.65 | N I | 40±15 ^c | 60 |
| | 1031.17 | 953.97 | N I | ... | 62 |
| | 1051.25 | 972.54 | H I (Ly γ) | ... | 90 |
| | 1056.09 | 977.02 | C III | 253±15 | 96 |
| | 1068.79 | 988.77 | O I | 56±13 | 115 |
| | 1069.90 | 989.80/87 | N III/Si II | ... | 116 |
| | 1108.73 | 1025.72 | H I (Ly β) | ... | 145 |
| | 1115.85 ^d | 1031.93 | O VI | 78±16 | 151 |
| | 1120.21 | 1036.34 | C II | 97±11 | 155 |
| | 1149.22 | 1063.18 | FeII | ... | 171 |
| | 1171.72 | 1083.99 | N II | 85±13 ^e | 180 |
| 0.13225 | 1161.37 | 1025.72 | H I (Ly β) | 177±15 | 175 |
| 0.13541 | 1078.34 | 949.74 | H I (Ly δ) | 77±15 | 121 |
| | 1104.23 | 972.54 | H I (Ly γ) | 68±13 | 139 |
| | 1109.32 | 977.02 | C III | 57±10 ^f | 146 |
| | 1122.66 | 988.77 | O I | ... | 158 |
| | 1123.83 | 989.80/87 | N III/Si II | -4 ± 18 | 159 |
| | 1164.61 | 1025.72 | H I (Ly β) | 147±15 | 178 |
| | 1171.66 | 1031.93 | O VI | ... | 179 |
| | 1176.67 | 1036.34 | C II | -9 ± 18 | 181 |
| | 1178.12 | 1037.62 | O VI | 18±19 | 182 |
| 0.17651 | 1103.33 | 937.80 | H I (Ly ϵ) | 51±14 | 138 |

Table 4—Continued

| z_{abs} | Observed λ (Å) | Transition λ (Å) | Species Ident. | $W_r \pm 1\sigma$ error (mÅ) | nr. ^a |
|------------------|---------------------------|-----------------------------|--------------------|---------------------------------|------------------|
| | 1117.38 | 949.74 | H I (Ly δ) | 58±12 | 154 |
| | 1144.20 | 972.54 | H I (Ly γ) | 142±16 | 169 |
| | 1149.47 | 977.02 | C III | ... | 172 |
| | 1163.30 | 988.77 | O I | −11 ± 17 | 176 |

^aLine identification numbers appearing in Fig. 1.

^bSlight blending with a nearby feature may lead to additional error in W_r .

^cWhile we report an equivalent width for this line, it may actually arise from Galactic O VI λ 1031.93 at $v = -320$ km s^{−1}.

^dThe O VI feature appears to be offset by +110 km s^{−1} relative to the other lines in this system. It is implausible that the shifted feature arises solely from H₂ in the Galaxy – see endnote *f* that applies to line nr. 152 in Table 3.

^eAssumes that no O VI is present in the system at $z_{\text{abs}} = 0.13541$.

^fPossible contamination from a feature arising from Galactic C I, but it should be weaker than the other Galactic C I features (nrs. 161, 166 and 174) in Table 3.

Finally, after accounting for absorption features in the STIS spectrum that could arise from the systems identified in the FUSE spectrum, we found 4 features shortward of the quasar’s Ly α emission peak that remained without identifications. We provisionally recognize these as Ly α absorptions from additional systems at redshifts 0.01187, 0.01771, 0.05119, and 0.19045 that do not reveal themselves in the FUSE spectrum. Their weaker Ly β counterparts are all hidden by other lines of known origin. The combined random and systematic errors for the redshifts of these systems are about ± 0.0006 .

4.2. Equivalent Width Measurements

We measured the equivalent widths of Galactic and extragalactic lines that were not obviously blended with other features. At locations where there was a reasonable expectation that a line might be present but none was seen, we evaluated a formal measurement of the equivalent width that yielded a value (sometimes negative) that was comparable to or less than the error. These nondetections are useful for obtaining upper limits for the column densities of certain species. We used continuum levels defined by least squares fits of Legendre polynomials to intensities on either side of each line, following the methods described by Sembach & Savage (1992). The outcomes of the measurements for the rest frame of each system, $W_r = W_{\lambda, \text{obs}} / (1 + z_{\text{abs}})$, are given in Columns 3 and 5 of Tables 3 and 4, respectively. The listed 1σ errors reflect uncertainties arising from two effects: one is the possible deviation of the result that could arise from the uncertainty of the defined continuum level,⁷ and the other is the uncertainty produced by random noise for intensities within the wavelength interval of the line. These effects should be independent of each other, hence their magnitudes are added in quadrature to arrive at a final error estimate.

Actual deviations in the intensities away from the adopted continuum levels exceeded the noise amplitudes defined by the *FUSE* data reduction pipeline by factors ranging from 1.2 to 1.4. We expect these increased errors arise from small, unrecognized absorption features or uncalibrated detector fixed-pattern noise. For our estimates of the contributions by random noise to the equivalent width errors, we used these larger excursions instead of error values supplied by the data reduction pipeline.

⁷We followed the practice of Jenkins (2002) of doubling the formal result for the continuum uncertainty, see §4.3 of his paper.

Table 5. Extragalactic Ly α Lines

| z_{abs} | Heliocentric λ (Å) ^a | W_r (Å) |
|------------------------------------|--|----------------------------|
| 0.01187 | 1230.1±0.6 | 0.24±0.05 |
| 0.01771 | 1237.2±0.5 | 0.21±0.06 |
| 0.05119 | 1277.9±0.5 | 0.60±0.05 |
| 0.07344 | 1305.0 | < 1.23 ± 0.06 ^b |
| 0.07779, 0.07900, 0.08093 | 1311.7 | 1.73±0.07 |
| 0.13225, 0.13541 | 1378.4 | 0.80±0.08 ^c |
| 0.17651 | 1430.3 | 0.38±0.04 |
| 0.19045 | 1447.2±0.7 | 0.09±0.03 |

^aSystems identified only by the appearance of Ly α features in the G140L STIS spectrum have their random wavelength uncertainties listed. Possible systematic errors (common to all lines) of up to 0.5 Å should be added in quadrature to these errors. We have not specified errors for systems with lines detected in the FUSE spectrum because the FUSE measurements are considerably more accurate (see §2.1).

^bThis measured value is actually an upper limit because there is interference from Galactic O I λ 1302.17 and Si II λ 1304.37.

^cLines are partly blended. Approximate contributions of $z_{\text{abs}} = 0.13225$ and 0.13541 components are 0.49 and 0.31 Å, respectively.

Table 6. Near-UV Lines

| z_{abs} | Observed λ (Å) | Transition λ (Å) ^a | Species Ident. | $W_r \pm 1\sigma$ error (mÅ) | nr. ^b |
|------------------|---------------------------|--|-------------------|---------------------------------|------------------|
| 0.0 | 2794.49 | 2796.35 | Mg II | 307±31 | 1 ^c |
| | 2796.35 | 2796.35 | Mg II | 904±42 ^d | 2 |
| | 2801.66 | 2803.53 | Mg II | 250±39 | 3 ^c |
| | 2803.53 | 2803.53 | Mg II | 785±42 | 4 |
| | 2852.96 | 2852.96 | Mg I | 234±28 | 6 |
| 0.08093 | 2810.60 | 2600.17 | Fe II | 172±24 | 5 |
| | 3022.66 | 2796.35 | Mg II | 145±53 | ... ^e |
| | 3030.42 | 2803.53 | Mg II | 162±53 | ... ^e |
| | 3083.85 | 2852.96 | Mg I | 137±60 | ... ^e |

^aVacuum wavelengths

^bLine identification numbers appearing in Fig. 4

^cGalactic component at a radial velocity $v \approx -200$ km s⁻¹.

^dSome contribution to this line's W_r may come from the Fe II $\lambda 2586.65$ line in the system at $z = 0.08093$.

^eSee upper panel of Fig. 3.

Measurements of the equivalent widths (and 1σ errors) of extragalactic Ly α features in the G140L STIS spectrum are listed in Table 5. In addition, equivalent widths of useful lines appearing in the near-UV STIS spectra shown in Figs. 3 and 4 are presented in Table 6. As with Tables 3 and 4, the last column of this table lists a numbered sequence for the features that appear in the spectrum (Fig. 4).

4.3. Galaxy Redshifts

Now having recognized the information about absorption systems available from the UV spectra, we move on to find possible links with galaxies observed from the ground, as described in §3. Unfortunately, no radial velocity standards could be taken during the APO observations of the galaxy spectra, so we used the spectrum of the standard star HD 182572 which had been taken at a different telescope. Although a radial velocity standard should ideally be obtained using the same instrument as the data whose redshifts are to be determined, the IRAF routine `fxcor` is able to resample spectra taken at different dispersions and compute a Fourier cross-correlation between the template spectrum and the object whose redshift is to be determined.

The results are given in Table 7. The numerical assignments given in column 1 are arbitrary and merely reflect the position of the object in the catalog of objects generated by `sextractor` (§3.1). We list the position and magnitude of the observed object as derived from the `sextractor` catalog in columns 2 and 4, along with the separation of the object from the sightline to PHL 1811 on the plane of the sky in arcsecs (column 3) and in h_{70}^{-1} kpc⁸ (column 7) based on the derived redshift (column 5). Measurement of a galaxy’s position and hence its distance from the sightline toward the quasar is derived from recalculating the barycenter of the CCD pixels comprising the galaxy, and can be measured to an accuracy better than 0.5 pixels (or 0''.2). At a redshift of 0.0809, this uncertainty corresponds to $0.3 h_{70}^{-1}$ kpc. A simple conversion of the observed magnitude to an absolute magnitude is given in column 8, with no k -correction. Redshift errors from `fxcor` are based on the fitted peak height and the antisymmetric noise as described by Tonry & Davis (1979), and are listed as $\sigma(z)$ in column 6 of Table 7. The value of $\sigma(z)$ depends on the S/N of the galaxy spectrum and on which absorption features are in common with the template spectrum. Since the galaxy spectra obtained at APO are of different quality from each other, and show different absorption features, the values of $\sigma(z)$ vary for each galaxy.

⁸ $h_{70} = H_0/70$, where H_0 is the Hubble constant, and $q_0 = 0$ is assumed throughout this paper.

Table 7. Spectroscopic Observations of Objects towards PHL 1811

| ID ^a | Galaxy or Star | | ρ^b ($''$) | R^e (4) | z (5) | $\sigma(z)^c$ (km s $^{-1}$) (6) | ρ^d (h_{70}^{-1} kpc) (7) | $(M_R$ (8) | Nearest z_{abs} (9) | Δv^g (km s $^{-1}$) (10) |
|-----------------|----------------|--------------------|----------------------|--------------|---------------------|---|---|---------------|------------------------------------|---|
| | ID | RA and DEC (J2000) | | | | | | | | |
| (1) | (2) | (3) | (4) | (5) | (6) | (7) | (8) | (9) | (10) | |
| G142 | 21:55:01.32 | –9:22:30.9 | 7.2 | 19.0 | 0.1917 | 210 | 22 | –20.8 | ... | ... |
| S144 | 21:55:01.53 | –9:22:04.5 | 19.8 | 16.6 | 0.0 | ... | ... | ... | ... | ... |
| S137 | 21:55:02.57 | –9:22:11.0 | 20.4 | 18.5 | 0.0 | ... | ... | ... | ... | ... |
| S143 | 21:55:01.78 | –9:22:03.6 | 21.1 | 18.0 | 0.0 | ... | ... | ... | ... | ... |
| G158 | 21:54:59.98 | –9:22:24.8 | 22.9 | 17.0 | 0.0808 | 100 | 34 | –20.8 | 0.08093 | –36 |
| S133 | 21:55:02.53 | –9:22:52.7 | 31.9 | 17.2 | 0.0 | ... | ... | ... | ... | ... |
| G151 | 21:55:00.58 | –9:22:50.0 | 29.3 | 19.4 | 0.1927 | 185 | 90 | –20.4 | ... | ... |
| G169 | 21:54:58.73 | –9:23:06.2 | 58.9 | 16.7 | 0.0804 | 60 | 88 | –21.1 | 0.08093 | –147 |
| G82 | 21:55:06.56 | –9:23:25.5 | 96.2 | 17.4 | 0.1322 | 250 | 220 | –21.5 | 0.13541 | –850 |
| G209 | 21:54:54.94 | –9:23:31.2 | 118.3 | 17.9 | 0.1761 | 100 | 340 | –21.7 | 0.17651 | –104 |
| G102 | 21:55:05.12 | –9:24:25.6 | 132.3 | 20.0 | 0.1582 ^h | ... | 350 | –19.5 | ... | ... |

^a “G” = galaxy; “S” = star.

^bSeparation between galaxy and PHL 1811 on the plane of the sky, in arcseconds.

^cApproximate error in redshift measurement from the cross-correlation analysis procedure **fxcor**.

^dImpact parameter between galaxy and PHL 1811 sightline, in h_{70}^{-1} kpc, where $h_{70} = H_0/70$, H_0 is the Hubble constant, and $q_0 = 0$.

^e R -band magnitude from the CCD frame shown in Fig. 5.

^fAbsolute magnitude of galaxy, with no k -correction.

^gError is dominated by the effect of $\sigma(z)$ (col. 6).

^hAll redshifts are measured from the cross-correlation of galaxy absorption features with a radial velocity standard, except G102, which has z derived from an [O II] $\lambda 3727$ emission line and hence there is no formal error from the cross-correlation analysis.

All of the galaxies observed showed the usual 4000 Å break along with Ca II H & K lines. G82 also showed an [O II] $\lambda 3727$ emission line, while G142 had [O II], H α , and [N II] $\lambda 6583$ emission lines present, but no H β and only a very weak [O III] $\lambda 5006$ line (the $\lambda 4958$ line being swamped by a sky emission line). G151 also showed [O II], H α , [N II] and weak [S II] $\lambda\lambda 6716, 6730$, while G102’s redshift was measured from a strong [O II] line; although the 4000 Å break and a weak [O III] $\lambda 5006$ line were visible, the signal-to-noise of the spectrum was too poor to provide a reliable redshift from cross-correlation with the template star.

Comparison of the galaxies for which we were able to obtain redshifts with all the galaxies cataloged suggests that we are likely complete in redshift information for non-stellar objects down to a magnitude of $R \approx 18.8$ at a radius of approximately $130''$. This corresponds to an absolute magnitude of $M_R - 5 \log h_{70} = -19.0$ ($0.3L^*$) and a radius of $179 h_{70}^{-1}$ kpc at the redshift of the $z = 0.08093$ LLS.

5. Properties of the Extragalactic Absorbing Systems

5.1. Lyman Limit System at $z_{\text{abs}} = 0.08093$

The absence of H₂ features or a very strong, damped Ly α absorption for the gas system at $z_{\text{abs}} = 0.08093$ (compare with the feature from our Galaxy in Fig. 2) suggests that the line of sight is probably not penetrating an arm within the inner disk of a galaxy. In fact, this system is probably associated with the outer portions of a galaxy, to be discussed later in §6.1, that has a virtually identical redshift at a projected distance of $23''$ from PHL 1811. Some O VI seems to be present, as evidenced by an absorption close to the redshifted transition at 1031.93 Å (line nr. 151 in Fig. 1 and Table 4), but at a velocity shift of about $+110 \text{ km s}^{-1}$ relative to the other gas. We are unable to confirm this identification by sensing the weaker 1037.62 Å line, which should appear at 1121.59 Å with an equivalent width of about 39 mÅ (or less, if there is some contamination of the 1032 Å line from the Galactic H₂ Lyman 0–0 P(3) line; see endnote *f* of Table 3). This longer wavelength member of the doublet might be too weak to detect above the noise, and it is partly blocked by Galactic Fe II at 1121.97 Å (line nr. 156 – this transition is about twice as strong as the another Fe II transition at 1125.45 Å, seen as line nr. 160, so the former should be stronger than the latter by an amount that depends on the line saturation).

The amount of H I present in the system is not well constrained. The fact that less than about 15% of the flux from PHL 1811 is transmitted below 988 Å defines a lower limit $N(\text{H I}) > 3 \times 10^{17} \text{ cm}^{-2}$. We are reluctant to make this limit more stringent because of

uncertainties in the *FUSE* scattered light determinations. The lack of any damping wings in excess of 10% absorption at 0.6\AA from the center of Ly β (line nr. 145) indicates that $N(\text{H I}) < 3 \times 10^{19}\text{cm}^{-2}$, a hundred times higher than our lower limit. Intermediate members of the Lyman series are not useful in further constraining the range, since they are on the flat portion of the curve of growth. *HST* observations of the Ly α transition at moderate resolution might reveal damping wings and thus give a direct determination of $N(\text{H I})$.

A problem of high priority in astrophysics, but one that is usually very difficult to carry out, is the measurement of the ratio of D I to H I in extragalactic and Galactic gas systems. The findings have important implications for our assessment of the total baryon density in the universe (Boesgaard & Steigman 1985; Walker et al. 1991), but this goal has been elusive because various determinations seem to disagree with each other (and weaknesses in some have been pointed out: Lemoine et al. 1999; Moos et al. 2001; O'Meara et al. 2001; Pettini & Bowen 2001). We now ask, “Can we measure D/H in the system at $z_{\text{abs}} = 0.08093$ in front of PHL 1811?” Obviously we are unable to do so at the moment because we do not know the value of $N(\text{H I})$ to within a full 2 orders of magnitude. Nevertheless, it is useful to examine whether or not this problem is tractable in the future, perhaps after *HST* observations of Ly α define $N(\text{H I})$ with reasonable accuracy and much longer observations have been carried out with *FUSE*.

Features from foreground Galactic H₂ make the sensing and measurement of Lyman series D I features in the $z_{\text{abs}} = 0.08093$ system very difficult. The strongest such line that is completely free of interfering H₂ absorptions is Ly ζ at $\lambda_{\text{obs}} = 1006.03\text{\AA}$ (line nr. 27). If $N(\text{H I})$ is equal to our upper limit of $3 \times 10^{19}\text{cm}^{-2}$, the deuterium feature at Ly ζ would have a strength of only 24 m\AA if $\text{D/H} = 2 \times 10^{-5}$. Here, the D feature would be measurable only under the extremely optimistic circumstances that $N(\text{H I})$ is large and the S/N is much better than what we have here. There are many absorption features on top of other high members of the Lyman series, such as Ly θ , Ly η , Ly ϵ , Ly δ and Ly γ (line nrs. 15, 19, 44, 57, and 90) but the relatively weak Lyman 0–0 R(0) and R(1) lines (nrs. 143 and 144) on top of Ly β could be modeled by studying the appearance of the 1–0 counterparts (nrs. 128 and 129) which are about 3.4 times as strong. In order to do this, one would need to determine the degree of saturation of the stronger pair of lines. However, even if we assume the saturation is very large (i.e., that the 0–0 lines are as strong as the 1–0 ones), we find that the absorption precisely on top of the expected position of the deuterium feature should not be very strong (but it is strong on either side of this location). The measured flux at this position in the *FUSE* data currently available is less than about 10% of the local continuum, so D I absorption at Ly β might be rather strong. However, in view of the fact that we are unable to identify a real “feature” at this location, we are reluctant to attribute this absorption to deuterium.

The O I $\lambda\lambda$ 988.77, 988.65, 988.58 blend (line nr. 115 in Fig. 1 and Table 4) appears to be not strongly saturated, since it is weaker than lines produced by either C II (nr. 155) or N II (nr. 180, but see endnote *e* of Table 4). If we assume these lines are near the linear portion of the curve of growth and adopt the combined *f*-value 0.0554 (Morton 2000), we arrive at $\log N(\text{O I}) = 14.07$, with an error in the linear value that scales in proportion to the listed uncertainty in equivalent width. Unfortunately, we cannot do the same for the N I λ 953.65 feature, which appears at 1030.83 Å, because there is a good chance that this feature is actually Galactic O VI at $v = -320 \text{ km s}^{-1}$ (Sembach et al. 2002). Other N I lines well removed from Galactic O VI are weaker and should be below our detection limit.

An absorption feature from Fe II λ 2600 is clearly detected in the STIS G230MB spectrum (line nr. 5 in Fig. 4 and Table 6). We find that $\log N(\text{Fe II}) \geq 13.05$ for an *f*-value of 0.224 (Morton 1991), with the actual number representing virtually no saturation of the line.⁹ The value of W_λ/λ for this line is not much different from that of O I feature discussed above, hence it is reasonable to compare O I to Fe II even if the lines are mildly saturated. We find that $\log N(\text{Fe II})/N(\text{O I}) = -1.02$, a value that is not very far from the solar value of -1.24 dex (Allende Prieto, Lambert, & Asplund 2001; Holweger 2002), indicating that the depletion by dust-grain formation is considerably less than the typical value of -1.4 dex found for warm gas in the disk of our Galaxy (Jenkins, Savage, & Spitzer 1986) or even -0.6 to -1.0 dex for lines of sight toward stars in the lower portion of the halo of our Galaxy (Savage & Sembach 1996; Sembach & Savage 1996). Of course, another alternative might be that depletion compensates for a fundamental overabundance of Fe with respect to O.

5.2. Other Systems

The most conspicuous features in the remaining systems that we identified are the Lyman series lines and the often very strong C III λ 977 line. Two of the systems, ones at $z_{\text{abs}} = 0.07900$ and 0.13225 , can be seen only at Ly β (line nrs. 141 and 175, respectively, in Fig. 1 and Table 4) in the *FUSE* spectrum. Attempts to find other strong lines, either to substantiate or discredit these identifications, failed because they were blocked by foreground Galactic features. If these features are not Ly β at the specified redshifts, then they must be deemed to be truly unidentified (they cannot be higher Lyman series lines at a higher redshift, otherwise the stronger and slightly weaker lines would also be visible). A reassurance

⁹Unfortunately, we are unable to verify that this line is unsaturated by examining the weaker λ 2586.65 transition, because the expected position of this line at 2795.86 Å is buried under the left-hand side of the Galactic Mg II transition at 2796.35 Å.

about the reality of the system at $z = 0.13225$ arises from a distinct feature at the expected wavelength 1376.4Å of Ly α in the STIS G140L spectrum (Fig. 2 and Table 5) and an almost exact match in the redshift of a galaxy (G82) reported in §4.3. We have not identified a galaxy near the redshift of the system at $z = 0.07900$, and the expected position of its Ly α feature is sandwiched between those of two other systems.

There seems to be no evidence in the form of Lyman series or C III $\lambda 977$ absorption that there is a distinct associated absorber system very near the redshift of PHL 1811. However, a very weak Ly α absorption is evident in the STIS G140L spectrum at $z = 0.19045$.

Accumulating evidence indicates that O VI absorbers harbor an important fraction of the baryons at low redshifts (Tripp, Savage, & Jenkins 2000; Tripp et al. 2001; Savage et al. 2002a). However, the current sample of low- z O VI systems is still rather small, and additional observations are needed to reduce statistical uncertainties. The PHL 1811 *FUSE* spectrum has sufficient resolution and S/N ratios to reveal isolated lines with $W_r \gtrsim 75$ mÅ at the 3σ level or better and is therefore useful for detecting potential O VI systems. Consequently, we searched the *FUSE* spectrum for systems that might be conspicuous only by absorption from the O VI doublet. No pairs of features with the correct spacing and intensity ratio for the O VI doublet were unambiguously apparent. Even if we assume the 1038 Å line is too weak to be seen (or is hidden by another line), we were unable to find single, unidentified lines with $W_r > 75$ mÅ in spectral regions where the probable equivalent width errors are less than 30 mÅ. However, the PHL 1811 spectrum is severely blanketed by H₂ and other Galactic absorption lines as well as extragalactic lines (see Tables 3 and 4), and this substantially reduces the “clear” redshift path available for detection of O VI. We estimate that in our *FUSE* spectrum the unblocked redshift path for identifying the 1032 Å O VI line is $\Delta z \approx 0.064$. Using the sight lines considered by Savage et al. (2002a), we derive a density $dN/dz = 9^{+8}_{-4}$ for the number of O VI $\lambda 1032$ lines per unit redshift with $W_r \geq 75$ mÅ. Therefore, we expect to find no more than about one O VI $\lambda 1032$ line in the PHL 1811 spectrum. Although we were unable to unambiguously identify *both* lines of the doublet at any redshift, the best identification of a significant line in Table 4 is O VI $\lambda 1032$ near the redshift of the LLS (line nr. 151).¹⁰ It therefore appears that our PHL 1811 findings are generally consistent with the results of previous studies of O VI systems.

¹⁰The $\lambda 1038$ line corresponding with line nr. 151 is difficult to measure due to blending with Galactic Fe II absorption. Another candidate line, nr. 148 associated with the system at $z = 0.07779$, represents a marginal detection below our conservative 75 mÅ threshold.

6. Relationships between Galaxies and Absorption Systems

6.1. Galaxy G158 at $z = 0.0808$

The galaxy we designate as G158 is at a redshift of $z = 0.0808$ and lies only $34 h_{70}^{-1}$ kpc from the line of sight of PHL 1811. We have been able to measure an R -band magnitude of $R = 17.0$, or $M_R - 5 \log h_{70} = -20.8$. The galaxy therefore has a luminosity of $\simeq L^*$ [assuming $M_R^* = -21.0 \pm 0.4$ from Lin et al. (1996)] and its major axis is aligned perpendicular to the sightline (see Fig. 5). It is obviously tempting to directly associate this absorber with the LLS at $z = 0.08093$, and below we discuss how the absorbing gas may be related to the galaxy. The association is particularly intriguing, given that the absorption is likely to arise in a multiphase medium, since it shows, e.g., C II, N II Mg II, and O I, as well as C III and, possibly, O VI (Table 4).

We begin by looking at the Mg II $\lambda\lambda 2796, 2803$ lines of the LLS, since much is already known about the absorbing galaxies identified with Mg II systems at $z \sim 0.5$. Mg II is detected in the G230L STIS spectrum of PHL 1811 at a redshift of 0.08093 with rest equivalent widths of $W_r(\lambda 2796) = 145 \pm 53$ mÅ and $W_r(\lambda 2803) = 162 \pm 53$ mÅ (see Table 6). Mg I $\lambda 2850$ is also marginally detected, with $W_r(\lambda 2850) = 137 \pm 60$ mÅ. After the initial detections of Mg II absorbing galaxies (Bergeron 1986; Cristiani 1987), more extensive surveys have led to the conclusion that all galaxies should have Mg II absorbing cross-sections of radii

$$R = R^* \left(\frac{L}{L^*} \right)^\beta \quad (1)$$

for systems with rest-frame equivalent width limits $W_r(\lambda 2796) \geq 0.3$ Å. The values of R^* and β depend on the color in which the galaxies are observed, but the differences are small, with $R^* = 50 h_{70}^{-1}$ kpc, $\beta = 0.2$, for galaxies with B -band luminosities and $R^* = 54 h_{70}^{-1}$ kpc, $\beta = 0.15$, for galaxies measured in the K -band (Steidel 1995). We do not have B -band magnitudes for our galaxies, but we can assume that the halo size-luminosity relationship for galaxies in the R -band is close to that in the B -band. We would then predict that the Mg II absorbing radius would be $\simeq 50 h_{70}^{-1}$ kpc. In fact, the equivalent widths of the Mg II lines at $z = 0.08093$ towards PHL 1811 are less than the $W_r \geq 0.3$ Å limit for the high- z Mg II absorbing galaxies. For weaker lines, the fiducial radius of an absorbing galaxy may increase from $50 h_{70}^{-1}$ kpc to more than $85 h_{70}^{-1}$ kpc, depending on the properties of the population of absorbers giving rise to the weak lines (Churchill et al. 1999). Clearly then, the higher redshift data indicate that we should indeed detect Mg II at the observed radius of $34 h_{70}^{-1}$ kpc for G158.

Although the size of the intermediate redshift Mg II absorbers has been examined in detail, the exact origin of the absorption is still under investigation, and numerous explana-

tions have been suggested to account for the data. For example, Steidel et al. (2002) have recently contributed to the notion that extended, diffuse galactic disks might explain the Mg II systems (Wagoner 1967; Bowen 1991; Lanzetta & Bowen 1992; Charlton & Churchill 1996, 1998; Churchill & Vogt 2001). They find evidence that the thick co-rotating disks of identified Mg II absorbing galaxies whose major axes are closely pointing towards a QSO sightline can explain the kinematical substructure of the absorption complexes.

Towards PHL 1811, we can examine whether the disk of G158 might also be responsible for the LLS absorption, using a prescription such as that given by Rubin et al. (1987). The axial ratio of G158 is ~ 1.54 which gives an inclination of $i \simeq 51^\circ$, while the angle between the major axis of the galaxy and the sightline is 89° . On the one hand, the sightline to PHL 1811 passes very close to the extension of the galaxy’s minor axis, and we would expect the velocity of the absorption to be close to the systemic velocity. Indeed, we find this to be the case, at least to the precision with which we are able to measure the redshift of G158. We also expect to see little or no kinematic substructure in the metal lines, again because the sightline intercepts material with a radial velocity component along the sightline of zero km s^{-1} . In keeping with this model, Figure 1 shows that the lines comprising the LLS show little complexity, at least on scales larger than the $\sim 20 \text{ km s}^{-1}$ resolution of the data.

On the other hand, given the inclination of G158 to the sightline, if a galaxy disk were responsible for the absorption, then it would have to have a projected radius of $\simeq 54 h_{70}^{-1} \text{ kpc}$ in order to intercept the sightline. This may be too large for even a gas-rich L^* galaxy: such a galaxy should have an H I radius at a limiting column density of $\log N(\text{H I}) = 19.0$ of $\simeq 31 h_{70}^{-1} \text{ kpc}$ (Bowen, Blades, & Pettini 1995). We know from the presence of the Lyman limit absorption and the lack of damping wings in the profile of the Ly β line that the H I column density is in the range $\log N(\text{H I}) \simeq 17.5 - 19.5$. Neutral hydrogen in galaxy disks is expected to be sharply truncated, extending perhaps only 10% further between $\log N(\text{H I}) = 19.0$ and 17.0 (Maloney 1993). Hence for G158, these models suggest that a drop in $\log N(\text{H I})$ with radius of 2 dex may not leave a high enough H I column density at a projected radius of $\simeq 54 h_{70}^{-1} \text{ kpc}$ (compared to the observed value). Still, extended H I disks with $\log N(\text{H I}) \geq 18$ and radii many times the optical extent of galaxies have been known for some time [see, e.g. Fig 1 of Hibbard et al. (2001)¹¹] and an extended gaseous disk may be a plausible explanation for the observed absorption.

There are several other possibilities to explain the origin of the absorbing material. Gas may arise in a dwarf satellite which lies directly along the sightline but which cannot be resolved in our image. Or perhaps gas produced from previous episodes of star formation

¹¹Also <http://www.nrao.edu/astrores/HIrogues/Rogues.html>

and deposited by galactic outflows may be situated in the same dark matter structures that the galaxy inhabits. Also, there could be dynamic stripping via interactions with other galaxies. It is of interest to note that there exists a second L^* galaxy at almost an identical redshift to G158 and the absorption system, namely G169, which lies $87 h_{70}^{-1}$ kpc from the PHL 1811 sightline. It is possible therefore that the line of sight passes through a group of galaxies, and that the absorbing material could be intragroup gas, or perhaps more directly, tidal debris which exists from a previous encounter between G158 and G169. Indeed, there is some evidence in Figure 5 for some extended emission to the south-east of G169 which might indicate a disturbed stellar population. A deeper image of the field is clearly needed to investigate this further. The redshifts of G158 and G169 as given in Table 7 differ by 110 km s^{-1} , but there is an error of ~ 60 and 100 km s^{-1} on the estimate of each of the redshifts. Since the signal-to-noise of both galaxy spectra are high, we can also cross-correlate the spectra with each other, to better estimate the velocity difference between the two galaxies. Again using the IRAF routine `fxcor`, we derive a difference in radial velocity of $190 \pm 80 \text{ km s}^{-1}$. This value is consistent with examples of two galaxies undergoing interactions in the local universe.

The metal lines of the $z = 0.08093$ system are not particularly complex, as might be expected from tidal debris distributed over several hundred km s^{-1} [e.g., Bowen et al. (1994)]. Nevertheless, the sightline to PHL 1811 need not pass through the bulk of the detritus, but could skirt the outlying regions of a tidal tail. Also, other absorption systems lie nearby in velocity, and these could in principle arise from tidal debris. Relative to the $z = 0.08093$ absorber, the $z = 0.07900, 0.07779$ and 0.07344 systems have velocity differences of $\Delta v = c\Delta z/(1+z) = -535, -870$ and -2077 km s^{-1} . Theoretical models of tidal tails in interacting pairs suggest that tails are most readily formed when the dark matter potential of the galaxies is not too deep, so that the escape velocity of the gas is at most a few times the circular rotation speed of the galaxy (Dubinski, Mihos, & Hernquist 1999). Given that most galaxies have rotation curves extending out to 300 km s^{-1} , tidal debris with a velocity difference of $\sim 500 \text{ km s}^{-1}$ is not out of the question, particularly when there exist examples in the local universe where the total extent of H I detected at 21 cm [i.e. $\log N(\text{H I}) \gtrsim 18$] spans such a velocity range [e.g., NGC 4676 (Hibbard & van Gorkom 1996), or the Magellanic Stream (Wakker 2001)]. However, there are few unambiguous examples of tidal tails with velocity gradients of $\geq 900 \text{ km s}^{-1}$, so the presence of the other two absorption systems is much harder to understand in terms of tidal interactions. Of course, the velocity extent of H I debris with column densities below that detectable from 21 cm emission measurements is not known, and could be much larger for low $N(\text{H I})$ clouds.

Yet, the apparent congregation of three absorption systems within 900 km s^{-1} of the $z = 0.08093$ LLS, if not simply coincidental, may also suggest that these systems, as well as

the LLS itself, arise in structures associated with intragroup, or perhaps, intracluster gas. As noted above, our exploratory redshift survey has covered a cross-section with a radius of only $179 h_{70}^{-1}$ kpc, and there may be more group galaxies than the two identified outside this region. Galaxies within compact groups can have velocity dispersions of up to 1000 km s^{-1} [e.g., HCG 23 (Williams & van Gorkom 1995)], or can even be embedded in single H I clouds with velocity gradients of 400 km s^{-1} at H I column densities of $\sim 10^{19} \text{ cm}^{-2}$ [e.g., HCG 26 (Williams & van Gorkom 1995)]. Hence the velocity differences seen between the LLS and the two lower redshift absorbers could be explained in terms of intragroup gas from a compact group. Still, the galaxies comprising the group around PHL 1811 could be less compact and form a looser group or cluster. More extensive redshift information is needed to test this hypothesis.

Recently, Bowen et al. (2002) proposed that the strength of a low redshift Ly α line complex is governed principally by the density of galaxies along a sightline. Ly α lines are seen in the G140L spectrum from the LLS, but at a resolution of $\lambda/\Delta\lambda \sim 1000$, individual components at $z = 0.08093, 0.07900$ and 0.07779 are blended together. Nevertheless, the total rest-frame equivalent width of the three systems is $1.73 \pm 0.07 \text{ \AA}$, which Bowen et al. predict should mark the presence of a dense group of galaxies. We note that a Ly α line is possibly detected from the lowest redshift system at $z = 0.07344$; however, most of the observed line is more likely to be strong Milky Way O I $\lambda 1302.17$ and Si II $\lambda 1304.37$, which is expected at about the same wavelength.

6.2. Other galaxies in the field of PHL 1811

6.2.1. Galaxies with Redshifts at $\sim z(\text{QSO})$

G142 is at a redshift of 0.1917 and lies only $22 h_{70}^{-1}$ kpc from the QSO sightline. We detect no features in the FUSE spectrum at this redshift, but a weak Ly α line is visible in the STIS G140L spectrum at 1447.2 \AA , or $z = 0.19045$. Although in principle we might expect to see a rich absorption system from a galaxy so close to the sightline of PHL 1811, the redshift of the system is close to that of the QSO emission redshift. Hence, the galaxy could actually be behind the QSO, or be affected by the intense ionizing flux from PHL 1811 itself. If correctly identified as Ly α , the weakness of the line could be because the interstellar gas in the disk and/or halo of G142 is more highly ionized than in more typical intervening absorbing galaxies, or the line could simply arise in material associated with the QSO itself and have nothing to do with G142.

G142 is not alone in being at the same redshift as PHL 1811. G151 is at a redshift of

$z = 0.1927$, and lies only $90 h_{70}^{-1}$ kpc to the line of sight. This is likely to be a member of the group which PHL 1811 inhabits.

6.2.2. Galaxies with Redshifts $\ll z$ (QSO)

We have identified three other galaxies close to the line of sight of PHL 1811 which have redshifts lower than the QSO emission redshift. G82 is a $2L^*$ galaxy at a redshift of $z = 0.1322$, lying $220 h_{70}^{-1}$ kpc from the QSO sightline. Although the exact relationship between galaxies and Ly α lines at $z < 1$ remains controversial, detailed studies by Chen et al. (2001) (and references therein) claim that galaxies of all types are surrounded by Ly α absorbing halos of radii $260 h_{70}^{-1}$ kpc or less for Ly α equivalent widths $\geq 0.3 \text{ \AA}$. Hence weak Ly α absorption is expected from G82 if this conclusion holds true. The G140L spectrum in fact shows two partially blended Ly α lines at $z = 0.13225$ and 0.13541 ($\Delta v = 840 \text{ km s}^{-1}$) with rest-frame equivalent widths of $W_r = 0.49$ and 0.31 \AA , respectively. The detection of the first of these systems at the same redshift as G82 is therefore roughly consistent with the results obtained at higher redshift. We note however, that numerical simulations which model how galaxies and gas collapse together to form Large Scale Structure (LSS) show that the scatter is large in the relationship between the predicted Ly α equivalent width and the impact parameter of the nearest bright galaxy (Davé et al. 1999). G82 may therefore be simply a galaxy in a common dark matter envelope shared by the Ly α -absorbing cloud.

G209 is a $2L^*$ galaxy which lies $340 h_{70}^{-1}$ kpc from the QSO sightline. Again, given this large distance we do not expect to see strong ($\geq 0.3 \text{ \AA}$) Ly α absorption at the redshift of G209. In fact, a Ly α line is detected at $z = 0.17651$ with $W_r = 0.38 \pm 0.04 \text{ \AA}$, close to the redshift of G209 of $z = 0.1761$. On the one hand, if galaxies and absorption systems are directly related, the “real” absorber must lie closer to the line of sight and be currently unidentified. On the other hand, G209 and the Ly α absorption may only be related by sharing the same LSS.

Finally, G102 ($z = 0.1582$) is a $0.3L^*$ edge-on galaxy which should also fail to show Ly α absorption, since it lies $350 h_{70}^{-1}$ kpc from the sightline to PHL 1811. A line can be seen close to the expected redshift at 1408 \AA , but we actually identify it to be a blend of O I $\lambda 1302$ and Si II $\lambda 1304$ at the redshift of the LLS.

7. Galactic Features

7.1. Low Velocity Material

The imprint of many lines from the Lyman and Werner bands of H₂ from the $J = 0$ to 4 rotational levels dominate the spectrum of PHL 1811 below about 1110 Å (see Table 3). The column density of H₂ is difficult to estimate since lines out of $J = 0$ and 1 are strongly saturated, as indicated by the flatness of a curve of growth for lines spanning a factor of 4 in strength. To express a lower limit for $N(\text{H}_2)$, we note that if the weakest line out of $J = 1$ were not badly saturated, we would obtain a column density of about 10^{16} cm^{-2} . This number is probably well below the actual column density however.

The only atomic hydrogen feature from the Galaxy in the *FUSE* spectrum that is visible is Ly β (line nr. 56 in Fig. 1 and Table 3). This feature is very broad and nearly box-shaped, without any indications of damping wings. For this reason, it is difficult to determine $N(\text{H I})$ – a situation similar to our problem with the LLS at $z_{\text{abs}} = 0.08093$.

There is a strong feature (line nr. 64) at the position of the O VI transition at 1031.93 Å, also reported by Wakker et al. (2002) from the same *FUSE* exposure, but no obvious half-strength counterpart is seen at 1037.62 Å, aside from a depression of flux between two other features. Our identifications of extragalactic gas systems toward PHL 1811 lead to no alternative candidates for the absorption at the location of the O VI feature at low velocity. Savage et al. (2002b) report that $\log N(\text{O VI}) = 14.45$.

7.2. High Velocity Material

A high velocity cloud at $v = -200 \text{ km s}^{-1}$ is apparent in the strongest atomic lines we can view, C II $\lambda 1036$ (line nr. 67 in Fig. 1 and Table 3) and Mg II $\lambda\lambda 2796, 2804$ (nrs. 1 and 3 in Fig. 4 and Table 6). The low-velocity H I Ly β line is too broad to distinguish this feature, and the higher Lyman lines are obscured by the Lyman limit absorption by the $z_{\text{abs}} = 0.08093$ system. Strong lines of less abundant species are not evident at this velocity.¹²

The high velocity cloud may be associated with the widely scattered group of clouds called complex GCN [reviewed by Wakker (2001)] with velocities ranging from -200 to about -300 km s^{-1} in the same general region of the sky. Mkn 509, $17^\circ 5$ away from PHL 1811, shows absorption features at -283 and -227 km s^{-1} (Sembach et al. 1995, 1999) that are

¹²A line at the correct relative location to the strong Fe II $\lambda 1144.94$ line is *not* from the high velocity cloud. It is the Ly γ feature (line nr. 169 in Table 4) of the system at $z_{\text{abs}} = 0.17651$.

attributed to this complex.

The Mg II lines have transition probabilities that differ from each other by a factor of 2. Since our measured ratio of their equivalent widths is 1.22 in the high-velocity gas, they must be strongly saturated. Thus, we can assume that the weaker line has $\tau_0 \gtrsim 3$ (corresponding to a true doublet ratio $DR = 1.25$), which leads to $\log N(\text{Mg II}) \gtrsim 13.4$ and $b \lesssim 11 \text{ km s}^{-1}$. For an upper limit, one may assume that b is very small and the stronger line is on the damping portion of the curve of growth. With its measured equivalent width plus a $1-\sigma$ error, we find that $\log N(\text{Mg II}) < 16.1$. If we apply the upper limit for b from the Mg II lines to interpret the C II line recorded by FUSE, we find that the line's central optical depth is large: $\tau_0 \gtrsim 6.8$, which leads to a lower limit $\log N(\text{C II}) > 14.6$. Using the same argument that we applied for the strong Mg II line, we obtain $\log N(\text{C II}) < 16.9$. If we assume the gas has solar abundance ratios for Mg and C of 7.54 and 8.39 (on logarithmic scale where H=12.00) determined by Holweger (2002) and Allende Prieto, Lambert & Asplund (2002), respectively, we estimate that the neutral hydrogen column density $\log N(\text{H I}) = 17.9$ and 18.2 for the lower limits of $N(\text{Mg II})$ and $N(\text{C II})$. These column densities are at about the detection threshold of the Leiden-Dwingeloo 21-cm survey of Hartmann & Burton (1997). No high-velocity feature is seen in the direction nearest PHL 1811 ($l = 47.5$, $b = -45.0$), but it is possible that a small wisp of gas in front of the quasar could be diluted by the large telescope beam.

O VI profiles at high negative velocities have been identified by Wakker et al. (2002). One component of this complex has $\log N(\text{O VI}) = 13.85$ in the velocity interval $-360 < v < -295 \text{ km s}^{-1}$, while the other shows $\log N(\text{O VI}) = 14.38$ at velocities $-200 < v < -65 \text{ km s}^{-1}$ (Sembach et al. 2002). Unfortunately, as we pointed out in §5.1 these features coincide with the two strongest N I features in the LLS ($z = 0.08093$). At present, there is no way to resolve this ambiguity in the identification of the lines. However, it seems more plausible to assert that the lines arise from Galactic O VI at large negative velocities, since the nitrogen identification would require an overabundance $[\text{N}/\text{O}] \approx 1.1$ to apply to the LLS.

8. Summary and Conclusions

Our primary intent in performing a short, exploratory observation of PHL 1811 with *FUSE* was to learn if the object was bright enough to warrant further spectroscopic investigations. We found that the far-UV flux of this object in the *FUSE* wavelength band, $F_\lambda \approx 5 \times 10^{-14} \text{ erg cm}^{-2}\text{s}^{-1}\text{\AA}^{-1}$, compares favorably with extrapolations from longer wavelengths. In addition to showing that high S/N spectra of PHL 1811 can be attained in reasonable observing times for either *FUSE* or *HST*, the spectrum exhibits a diverse set of

intervening systems. We have here a case that promises benefits in understanding low- z gas systems that may measure up to the findings that have recently been derived from the brightest known quasar in the sky, 3C273 (Sembach et al. 2001; Tripp et al. 2002). A mildly disappointing but not unexpected result is that Galactic H₂ features in the *FUSE* spectrum result in the loss of many extragalactic lines. Even so, a total of 36 of them were free from blending at the 15 km s⁻¹ resolution of *FUSE*, and we could measure their equivalent widths (but in some cases the values were less than their errors). Moreover, high resolution observations at longer wavelengths with HST should overcome the problem of blockage from H₂ features.

Over a redshift path $\Delta z = 0.192$, we have identified 7 absorption systems at redshifts $z_{\text{abs}} = 0.07344, 0.07779, 0.07900, 0.08093, 0.13225, 0.13541$ and 0.17651 , plus another 4 possible systems that show only Ly α in our low resolution STIS spectrum. The 7 systems that we feel are securely identified, or groups thereof, show Ly α features with rest-frame equivalent widths in excess of about 300 mÅ. The normal expectation for finding such systems is about half the yield that we obtained, since the product of our Δz and general result $dN/dz = 18$ for $z \approx 0$ (Bahcall et al. 1993; Penton, Shull, & Stocke 2000) equals only 3.5. Likewise, we were very fortunate to find a Lyman limit system (the LLS at $z_{\text{abs}} = 0.08093$). For a random line of sight we would have had only a 6% chance of intercepting one, if we extrapolate the average number density of such systems measured by Stengler-Larrea et al. (1995) to $z \approx 0$, $dN/dz = 0.3$, and then multiply it by our Δz .

While the H I column density of the LLS is very uncertain, we were able to carry out rudimentary measurements of the amounts of O I and Fe II present, subject to the assumption that the absorption features are not strongly saturated. We interpret our finding that $[\text{Fe}/\text{O}] \approx 0.3$ to suggest that either there is little depletion of refractory elements by the formation of dust grains, or that if such depletion exists, it is approximately counterbalanced by an excess abundance of Fe compared that expected from solar abundances. Unfortunately, a coincidence in the expected positions of the strongest N I features with those of high-velocity Galactic O VI blocks our attempt to derive secure conclusions on the nitrogen abundance. However, we expect to be able to measure N abundances and compare them to O as soon as we obtain an *HST* observation of PHL 1811 using the STIS E140M grating.¹³ This observation will cover the 1200 Å multiplet of N I and the 1302 Å line of O I. These lines have f -values similar to the ones reported here for the *FUSE* spectrum, and the 3 lines of N I would offer guidance on the amount of saturation through a standard curve-of-growth analysis.

¹³Observations of PHL 1811 using the STIS E140M grating are currently scheduled for Cycle 11 (Program ID=9418).

From our imaging of the field around PHL 1811 coupled with spectroscopic measurements of galaxy redshifts, we conclude that the LLS at $z_{\text{abs}} = 0.08093$ in front of PHL 1811 is likely to be associated with an L^* galaxy (G158) which lies $34 h_{70}^{-1}$ kpc off the sightline. A second L^* galaxy (G169) at a similar redshift lies $88 h_{70}^{-1}$ kpc away, and may be interacting with the nearer galaxy. Absorption may arise in the disk of G158, although the disk would need to be much larger than would be typical for a galaxy of its luminosity. Absorption could arise in the halo of G158, but the existence of two other absorption systems within only 900 km s^{-1} of the LLS suggest that the galaxy and the system itself may be part of a larger structure, and that the absorption systems could be signatures of intragroup, or intracluster, gas.

The *FUSE* spectrum of PHL 1811 was obtained for the Guaranteed Time Team by the NASA-CNES *FUSE* mission operated by Johns Hopkins University. Financial support has been provided by NASA contract NAS5-32985 and support for writing this paper came from Contract 2440-60014 to Princeton University. Additional support was provided by a NASA LTSA grant NAG5-11136 to Princeton University. The acquisition of the G230MB spectrum was supported by an *HST* guest observer grant HST-GO-09128.01A.

REFERENCES

Abgrall, H., & Roueff, E. 1989, A&AS, 79, 313

Allende Prieto, C., Lambert, D. L., & Asplund, M. 2001, ApJ, 556, L63

— 2002, ApJ, 573, L137

Bahcall, J. N., Bergeron, J., Boksenberg, A., Hartig, G. F., Jannuzi, B. T., Kirhakos, S., Sargent, W. L. W., Savage, B. D., Schneider, D. P., Turnshek, D. A., Weymann, R. J., & Wolfe, A. M. 1993, ApJS, 87, 1

Bergeron, J. 1986, A&A, 155, L8

Boesgaard, A. M., & Steigman, G. 1985, ARA&A, 23, 319

Bowen, D. V. 1991, MNRAS, 251, 649

Bowen, D. V., Blades, J. C., & Pettini, M. 1995, ApJ, 448, 634

Bowen, D. V., Pettini, M., & Blades, J. C. 2002, ApJ, 580, 169

Bowen, D. V., Roth, K. C., Blades, J. C., & Meyer, D. M. 1994, ApJ, 420, L71

Charlton, J. C., & Churchill, C. W. 1996, ApJ, 465, 631

— 1998, ApJ, 499, 181

Chen, H.-W., Lanzetta, K. M., Webb, J. K., & Barcons, X. 2001, *ApJ*, 559, 654

Churchill, C. W., & Vogt, S. S. 2001, *AJ*, 122, 679

Churchill, C. W., Rigby, J. R., Charlton, J. C., & Vogt, S. S. 1999, *ApJS*, 120, 51

Cristiani, S. 1987, *A&A*, 175, L1

Davé, R., Hernquist, L., Katz, N., & Weinberg, D. H. 1999, *ApJ*, 511, 521

Dubinski, J., Mihos, J. C., & Hernquist, L. 1999, *ApJ*, 526, 607

Hartmann, D., & Burton, W. B. 1997, *Atlas of Galactic Neutral Hydrogen*, (Cambridge: Cambridge Univ. Press)

Hibbard, J. E., & van Gorkom, J. H. 1996, *AJ*, 111, 655

Hibbard, J. E., van Gorkom, J. H., Rupen, M. P., & Schimonovich, D. S. 2001, in *Gas and Galaxy Evolution*, ed. J. E. Hibbard, J. H. van Gorkom & J. H. Rupen (San Francisco: Ast. Soc. Pacific), p. 657

Holweger, H. 2002, in *Joint SOHO/ACE Workshop: Solar and Galactic Composition*, ed. R. F. Wimmer-Schweingruber (New York: AIP), p. 23

Jenkins, E. B. 2002, *ApJ*, 580, 938

Jenkins, E. B., Savage, B. D., & Spitzer, L. 1986, *ApJ*, 301, 355

Kerr, F. J., & Lynden-Bell, D. 1986, *MNRAS*, 221, 1023

Landolt, A. U. 1992, *AJ*, 104, 372

Lanzetta, K. M., & Bowen, D. V. 1992, *ApJ*, 391, 48

Leighly, K. M., Halpern, J. P., Helfand, D. J., Becker, R. H., & Impey, C. D. 2001, *AJ*, 121, 2889

Leitherer, C. 2001, *Space Telescope Imaging Spectrograph Instrument Handbook for Cycle 11*, 5.1 ed., (Baltimore: Space Telescope Science Institute), p. 455.

Lemoine, M., Audouze, J., Ben Jaffel, L., Feldman, P., Ferlet, R., Hébrard, G., Jenkins, E. B., Mallouris, C., Moos, W., Sembach, K., Sonneborn, G., Vidal-Madjar, A., & York, D. G. 1999, *New Astronomy*, 4, 231

Lin, H., Kirshner, R. P., Shectman, S. A., Landy, S. D., Oemler, A., Tucker, D. L., & Schechter, P. L. 1996, *ApJ*, 464, 60

Maloney, P. 1993, *ApJ*, 414, 41

Mihalas, D., & Binney, J. 1981, *Galactic Astronomy Structure and Kinematics*, 2nd ed., (New York: Freeman)

Monet, D. et al. 1996, *USNO-SA2.0*, (Washington: US Naval Obs.)

Moos, H. W. et al. 2000, ApJ, 538, L1

Moos, H. W. et al. 2001, ApJS, 140, 3

Morton, D. C. 1991, ApJS, 77, 119

Morton, D. C. 2000, updated version of Morton (1991) privately circulated to the *FUSE* investigation team.

O'Meara, J. M., Tytler, D., Kirkman, D., Suzuki, N., Prochaska, J. X., Lubin, D., & Wolfe, A. M. 2001, ApJ, 552, 718

Penton, S. V., Shull, J. M., & Stocke, J. T. 2000, ApJ, 544, 150

Pettini, M., & Bowen, D. V. 2001, ApJ, 560, 41

Rubin, V. C., Thonnard, N., & Ford, W. K. 1987, AJ, 87, 477

Sahnow, D. J. et al. 2000, ApJ, 538, L7

Savage, B. D., & Sembach, K. R. 1996, ApJ, 470, 893

Savage, B. D., Sembach, K. R., Tripp, T. M., & Richter, P. 2002a, ApJ, 564, 631

Savage, B. D., Sembach, K. R., Wakker, B. P., Richter, P., Meade, M., Jenkins, E. B., Shull, J. M., Moos, H. W., & Sonneborn, G. 2002b, astro-ph/0208140

Sembach, K. R., & Savage, B. D. 1992, ApJS, 83, 147

— 1996, ApJ, 457, 211

Sembach, K. R., Savage, B. D., Lu, L. M., & Murphy, E. M. 1995, ApJ, 451, 616

Sembach, K. R., Savage, B. D., Lu, L., & Murphy, E. M. 1999, ApJ, 515, 108

Sembach, K. R., Howk, J. C., Savage, B. D., Shull, J. M., & Oegerle, W. R. 2001, ApJ, 561, 573

Sembach, K. R., Wakker, B. P., Savage, B. D., Richter, P., Meade, M., Shull, J. M., Jenkins, E. B., Sonneborn, G., & Moos, H. W. 2002, astro-ph/0207562

Steidel, C. C. 1995, in QSO Absorption Lines, ed. G. Meylan (Berlin: Springer), p. 139

Steidel, C. C., Kollmeier, J. A., Shapley, A. E., Churchill, C. W., Dickinson, M., & Pettini, M. 2002, ApJ, 570, 526

Stengler-Larrea, E. A., Boksenberg, A., Steidel, C. C., Sargent, W. L. W., Bahcall, J. N., Bergeron, J., Hartig, G. F., Jannuzzi, B. T., Kirhakos, S., Savage, B. D., Schneider, D. P., Turnshek, D. A., & Weymann, R. J. 1995, ApJ, 444, 64

Tonry, J., & Davis, M. 1979, AJ, 84, 1511

Tripp, T. M., Savage, B. D., & Jenkins, E. B. 2000, ApJ, 534, L1

Tripp, T. M., Giroux, M. L., Stocke, J. T., Tumlinson, J., & Oegerle, W. R. 2001, *ApJ*, 563, 724

Tripp, T. M., Jenkins, E. B., Williger, G. M., Heap, S. R., Bowers, C. W., Danks, A. C., Davé, R., Green, R. F., Gull, T. R., Joseph, C. L., Kaiser, M. E., Lindler, D., Weymann, R. J., & Woodgate, B. E. 2002, *ApJ*, 575, 697

Wagoner, R. V. 1967, *ApJ*, 149, 465

Wakker, B. P. 2001, *ApJS*, 136, 463

Wakker, B. P. et al. 2002, *astro-ph/0208009*

Walker, T. P., Steigman, G., Kang, H.-S., Schramm, K. M., & Olive, K. A. 1991, *ApJ*, 376, 51

Williams, B. A., & van Gorkom, J. H. 1995, in *Groups of Galaxies*, ed. O.-G. Richter & K. Borne (San Francisco: Ast. Soc. Pacific), p. 77